USP21 negatively regulates antiviral response by acting as a RIG-I deubiquitinase

Yihui Fan,[1,3] Renfang Mao,[2] Yang Yu,[1] Shangfeng Liu,[3] Zhongcheng Shi,[5] Jin Cheng,[1] Huiyuan Zhang,[6] Lei An,[6] Yanling Zhao,[1] Xin Xu,[1] Zhenghu Chen,[3] Mari Kogiso,[1] Dekai Zhang,[5] Hong Zhang,[2,6] Pumin Zhang,[7] Jae U. Jung,[8] Xiaonan Li,[1] Guotong Xu,[3,4] and Jianhua Yang[1]

[1]Texas Children's Cancer Center, Department of Pediatrics, [2]Department of Pathology and Immunology, Dan L. Duncan Cancer Center, Baylor College of Medicine, Houston, TX 77030
[3]Translational Center for Stem Cell Research, Tongji Hospital, Department of Regenerative Medicine; [4]Department of Ophthalmology, Shanghai Tenth People's Hospital, and Tongji Eye Institute, Tongji University School of Medicine, Shanghai 200065, China
[5]Center for Infectious and Inflammatory Diseases at Institute of Biosciences and Technology, Texas A&M University Health Science Center, Houston, TX 77030
[6]Department of Pathology, MD Anderson Cancer Center, Houston, TX 77030
[7]Departments of Molecular Physiology and Biophysics, Baylor College of Medicine, Houston, TX 77030
[8]Department of Molecular Microbiology and Immunology, Keck School of Medicine, University of Southern California, Los Angeles, CA 90033

Lys63-linked polyubiquitination of RIG-I is essential in antiviral immune defense, yet the molecular mechanism that negatively regulates this critical step is poorly understood. Here, we report that USP21 acts as a novel negative regulator in antiviral responses through its ability to bind to and deubiquitinate RIG-I. Overexpression of USP21 inhibited RNA virus–induced RIG-I polyubiquitination and RIG-I–mediated interferon (IFN) signaling, whereas deletion of USP21 resulted in elevated RIG-I polyubiquitination, IRF3 phosphorylation, IFN-α/β production, and antiviral responses in MEFs in response to RNA virus infection. USP21 also restricted antiviral responses in peritoneal macrophages (PMs) and bone marrow–derived dendritic cells (BMDCs). USP21-deficient mice spontaneously developed splenomegaly and were more resistant to VSV infection with elevated production of IFNs. Chimeric mice with USP21-deficient hematopoietic cells developed virus-induced splenomegaly and were more resistant to VSV infection. Functional comparison of three deubiquitinases (USP21, A20, and CYLD) demonstrated that USP21 acts as a bona fide RIG-I deubiquitinase to down-regulate antiviral response independent of the A20 ubiquitin-editing complex. Our studies identify a previously unrecognized role for USP21 in the negative regulation of antiviral response through deubiquitinating RIG-I.

CORRESPONDENCE
Guotong Xu:
gtxu@tongji.edu.cn
OR
Jianhua Yang:
jianhuay@bcm.edu

Abbreviations used: BMDC, BM-derived dendritic cell; CARD, caspase recruitment domain; DUB, deubiquitinating enzyme; MEF, mouse embryonic fibroblast; PM, peritoneal macrophage; PRR, pattern recognition receptor; RLR, RIG-I-like receptor; SeV, Sendai virus; Ub, ubiquitin; USP21, ubiquitin-specific peptidases 21; VSV, vesicular stomatitis virus.

The innate immune system, an evolutionarily conserved mechanism, is the first line of defense against viral infection. The hallmark of antiviral innate immune response is induction of type I IFNs and proinflammatory cytokines (Yoneyama and Fujita, 2009; Takeuchi and Akira, 2010). Type I IFNs not only locally suppress viral infection and proliferation but also facilitate effective adaptive immune responses. Induction of type-I IFN is initiated by detection of viral nucleic acids through the pattern recognition receptor (PRRs) family, including TLRs, RIG-I–like receptors (RLRs), NOD-like receptors (NLRs), and C-type lectin receptors (CLRs; Akira et al., 2006). RLRs include RIG-I, MDA5, and LGP2, all of which contain a DExD-box RNA helicase domain, but only RIG-I and MDA5 contain N-terminal tandem caspase recruitment domains (CARDs) that mediate downstream signaling (Yoneyama et al., 2004; Fujita, 2009). RIG-I is essential for type-I IFN production in mouse embryonic fibroblasts (MEFs), conventional dendritic cells (cDCs), and macrophages in response to RNA viruses such as Sendai virus (SeV), vesicular stomatitis virus (VSV), hepatitis C virus (HCV), influenza A

The Rockefeller University Press $30.00
J. Exp. Med. 2014 Vol. 211 No. 2 313-328
www.jem.org/cgi/doi/10.1084/jem.20122844

virus (Flu), and Japanese encephalitis virus (JEV; Kato et al., 2005; Kato et al., 2006). Virus-induced IFN production is tightly regulated to prevent persistent IFN production, which has been associated with a variety of immunological disorders (Seth et al., 2005; Moser et al., 2009; Ramos et al., 2011).

Upon binding to RNA ligands, the conformation of the RIG-I protein changes and then the N-terminal tandem CARDs trigger interaction with its downstream partner MAVS (Kawai et al., 2005; Meylan et al., 2005; Seth et al., 2005; Xu et al., 2005). MAVS contains an N-terminal CARD that interacts with the tandem CARDs of RIG-I and a C-terminal trans-membrane domain that localizes it to the mitochondrial outer membrane. MAVS then activates IKKα–IKKβ–NEMO and TBK1–IKKε complexes, which in turn activate the transcription factors NF-κB and IRF3, respectively. Together with other transcription factors, NF-κB and IRF3 induce the expression of type I IFNs and other antiviral cytokines (Yoneyama and Fujita, 2009; Takeuchi and Akira, 2010). Lys63-linked polyubiquitination of RIG-I at Lys-172 catalyzed by TRIM25 is an important step for RIG-I activation (Gack et al., 2007). Another RIG-I E3 ligase, RNF135, mediates Lys63-linked polyubiquitination of RIG-I at the C-terminal domain and is essential for RIG-I–dependent immune responses (Gao et al., 2009; Oshiumi et al., 2009, 2010). An in vitro reconstitution system of the RIG-I pathway showed that unanchored Lys63-linked polyubiquitin chains binding to RIG-I is required for RIG-I activation (Zeng et al., 2010). Compared to Lys63-linked polyubiquitination-mediated RIG-I activation, the negative regulation of Lys63-linked polyubiquitination of RIG-I is less understood.

Ubiquitination, a reversible process, can be reversed by deubiquitinating enzymes (DUBs), which specifically cleave the isopeptide bond at the C terminus of ubiquitin (Ub; Komander et al., 2009). A20, an ubiquitin-editing enzyme, has been shown to negatively regulate antiviral pathways (Wang et al., 2004; Saitoh et al., 2005; Lin et al., 2006; Parvatiyar et al., 2010). However, due to the fact that the deubiquitinase activity of A20 is not required for its inhibitory effect in antiviral signaling, A20 is unlikely to act as a direct RIG-I deubiquitinase and the mechanism remains to be clearly defined (Lin et al., 2006; Parvatiyar et al., 2010). Another DUB family protein, CYLD, has been suggested as a RIG-I deubiquitinase to negatively regulate antiviral response (Friedman et al., 2008; Zhang et al., 2008). However, CYLD has also been shown to bind to and deubiquitinate TBK1 and IKKε (Friedman et al., 2008). A recent in vivo study reported that CYLD is required for host defense against VSV infection, suggesting the precise mechanism and the direct target(s) of CYLD in antiviral response remain to be clarified (Zhang et al., 2011). Therefore, the authentic deubiquitinase of RIG-I remains unclear.

Using a functional genomic screening, we have identified USP21 as a bona fide RIG-I deubiquitinase. USP21 inhibits virus-induced IRF3 activation via binding to and deubiquitinating RIG-I. Genetic deletion of USP21 in primary MEFs, peritoneal macrophages (PMs), and BM–derived dendritic cells (BMDCs) enhances virus- and RIG-I CARD domain (RIG-I-CARD)–induced IRF3 activation, IFN-α/β production, and antiviral response. Mice lacking USP21 are viable and fertile, but they present splenomegaly and are more resistant to VSV infection with elevated IFNs production. The inhibitory function of USP21 in antiviral signaling is independent of A20 ubiquitin-editing complex. Our results reveal the novel physiological function of USP21 in antiviral response and highlight USP21 as a RIG-I deubiquitinase.

RESULTS

USP21 inhibits RIG-I-CARD–mediated IRF3 activation and negatively regulates antiviral response

Lys63-linked polyubiquitination of RIG-I-CARD plays an essential role in RNA virus–induced IRF3 activation and IFN-β production (Gack et al., 2007). However, the molecular mechanism of RIG-I-CARD deubiquitination is not fully understood. To explore whether members of the ubiquitin-specific peptidase (USPs) subclass of DUBs are involved in the deubiquitination of RIG-I-CARD and down-regulation of RIG-I-CARD–mediated IRF3 activation, we screened a library of mammalian expression vectors that encode 37 USPs to assess the effects of overexpression of each USP on RIG-I-CARD–induced IFN-β luciferase activity. In this screening, USP18 and USP21 significantly inhibited RIG-I-CARD–induced IFN-β reporter activity, whereas other USPs had no effect or fewer effects (Fig. 1 A). USP18, an ISG15 deconjugating protease, has been suggested to negatively regulate antiviral response (Ritchie et al., 2004; Malakhova et al., 2006). USP21 is a highly conserved deubiquitinase and has a relatively high expression in immune organs and cells (unpublished data).

Next, we examined whether the deubiquitinase activity of USP21 is required for its inhibitory effect. Overexpression of USP21 WT, but not its deubiquitinase-deficient (C221A) mutant, blocked the SeV-, RIG-I-CARD–, and TBK1-induced IFN-β reporter activity (unpublished data). Because IFN-β reporter activity is dependent on both NF-κB and IRF3 (Honda et al., 2006), we further tested the inhibitory effect of USP21 on SeV-, RIG-I-CARD–, and TBK1-induced NF-κB and ISRE reporter activities. USP21 WT but not C221A mutant inhibited SeV-, RIG-I-CARD–, and TBK1-induced NF-κB reporter activity (unpublished data). However, USP21 only inhibited SeV- and RIG-I-CARD–, but not TBK1-induced ISRE reporter activity (Fig. 1, B–D). Consistently, USP21 WT but not C221A mutant inhibited RIG-I-CARD– but not MAVS- or TBK1-induced IRF3 phosphorylation (Fig. 1, E–G). Furthermore, human USP21 inhibited SeV-induced IFN-β reporter activities in MEFs whereas mouse USP21 inhibited SeV-induced IFN-β reporter activities in HEK293T cells (Fig. 1 H and not depicted), suggesting that USP21 function in antiviral signaling is not limited by cell type and is conserved between human and mouse.

Because IRF3 activation is critical for antiviral response, we determined whether USP21 could inhibit antiviral response. Ectopic expression of USP21 WT but not C221A mutant

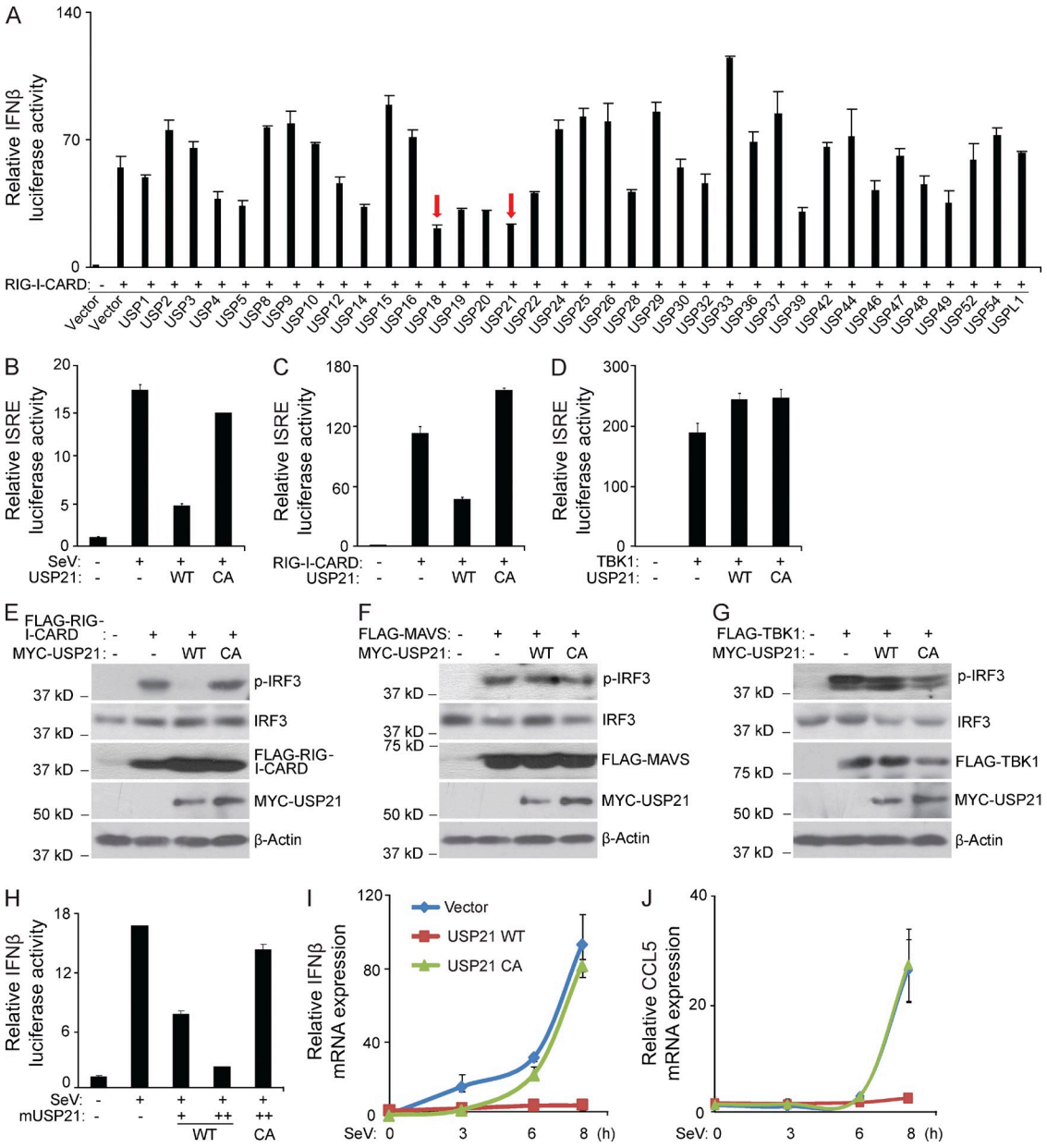

Figure 1. USP21 inhibits RIG-I-CARD–induced IRF3 activation and IFN-β signaling. (A) RIG-I-CARD was co-transfected with indicated USPs or control vectors along with IFN-β luciferase reporter into HEK293T cells for 36 h. IFN-β luciferase activity was measured and normalized with the *Renilla* activity. (B) HEK293T cells were transfected with USP21 WT or C221A (CA) mutant along with ISRE luciferase reporter vectors for 24 h, and then infected with SeV or left uninfected for 12 h before ISRE luciferase was measured. (C and D) RIG-I-CARD or TBK1 were co-transfected with USP21 WT or CA mutant along with ISRE luciferase reporter vectors into HEK293T cells for 36 h before ISRE luciferase activity was measured. (E–G) FLAG-RIG-I-CARD, FLAG-MAVS, or FLAG-TBK1 were co-transfected with empty vector or expression vector encoding MYC-USP21 WT or CA mutant into HEK293T cells for 36 h. Cells lysates were immunoblotted with the indicated antibodies. (H) HEK293T cells were transfected with mouse orthologous USP21 WT or CA mutant along with IFN-β luciferase vectors for 24 h, and then infected with SeV or left untreated for 12 h before luciferase was measured. (I and J) HEK293T cells were transfected with USP21 WT or CA mutant for 36 h, and then infected with SeV at the indicated time points. The mRNA level of IFN-β and CCL5 was measured by real-time RT-PCR. Error bars indicate ±SD in duplicate experiments. Data from A is a screening data from one experiment. Data are representative of two (H–J) or at least three (B–G) independent experiments.

blocked SeV-induced IFN-β and CCL5 production (Fig. 1, I and J). Consistently, ectopic expression of USP21 WT but not C221A mutant made cells more susceptible toVSV infection and failed to prevent VSV replication (unpublished data). These results suggest that USP21 is a novel negative regulator in antiviral response and very likely targets RIG-I.

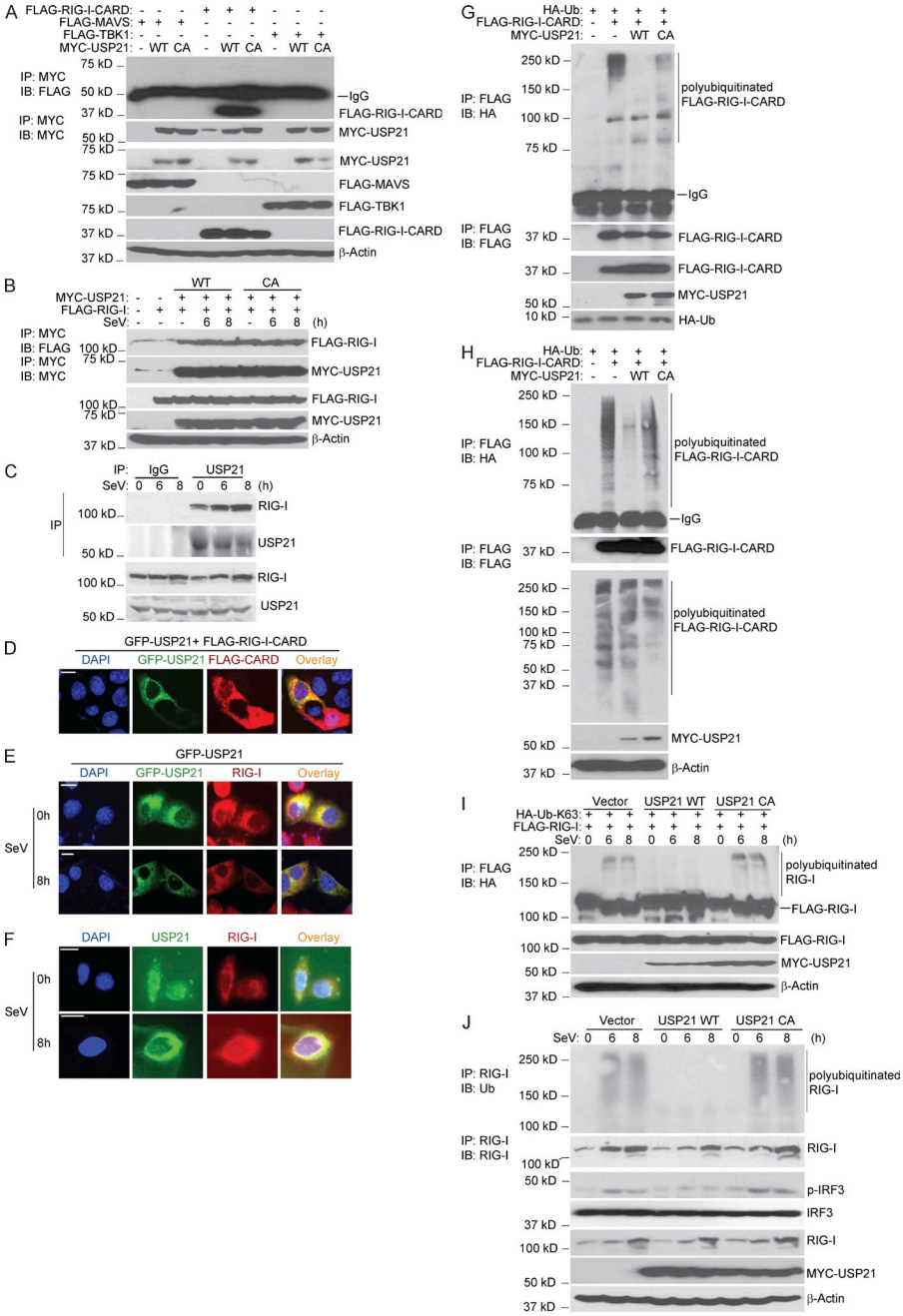

Figure 2. USP21 binds to RIG-I and deubiquitinates RIG-I. (A) HEK293T cells were transfected with MYC-USP21 WT or CA mutant along with FLAG-RIG-I-CARD, FLAG-MAVS, or FLAG-TBK1 for 36 h. Cell lysates were immunoprecipitated with anti-MYC antibodies and immunoblotted with anti-FLAG antibodies. (B) HEK293T cells were transfected with MYC-USP21 WT or CA mutant along with FLAG-RIG-I for 24 h, and then infected with SeV for the indicated time points. Cell lysates were immunoprecipitated with anti-MYC antibodies and immunoblotted with anti-FLAG antibodies. (C) HeLa cells were infected with SeV for the indicated time points. Endogenous USP21 in cell lysates were immunoprecipitated with anti-USP21 antibodies and immunoblotted with anti–RIG-I antibodies. (D) HeLa cells were transfected with GFP-USP21 and FLAG-RIG-I-CARD for 36 h, and then stained by anti-FLAG antibodies (red). Bar, 10 µm. (E) HeLa cells were transfected with GFP-USP21 for 36 h, and then left uninfected or infected with SeV for 8 h. immunofluorescent staining was performed with anti–RIG-I antibodies (red). Bar, 10 µm. (F) HeLa cells were left uninfected or infected with SeV for 8 h. Immunofluorescent staining was performed with anti-USP21 (green) and anti–RIG-I (red). Bar, 10 µm. (G) FLAG-RIG-I-CARD and HA-Ub were co-transfected into HEK293T cells with control or MYC-USP21 WT or CA mutant. Cell lysates were heated in the presence of 1% SDS and diluted with lysis buffer, and then immunoprecipitated with anti-FLAG antibodies and immunoblotted with anti-HA antibodies. (H) HEK293T cells were transfected with control, MYC-USP21 WT, or CA mutant and cell lysates were immunoprecipitated with anti-MYC antibodies. In the parallel experiments, HEK293T cells were transfected with FLAG-RIG-I-CARD and HA-Ub. Cells were lysed in the lysis buffer only with PMSF. Supernatant containing polyubiquitinated FLAG-RIG-I-CARD proteins were incubated with immunoprecipitated MYC-USP21 WT or CA mutant for 2 h at 30°C, and then immunoprecipitated with anti-FLAG antibodies and immunoblotted with anti-HA antibodies. (I) FLAG-RIG-I and HA-Ub-K63 were co-transfected into HEK293T cells with control, MYC-USP21 WT, or CA mutant. Transfected cells were infected with SeV for the indicated time points. Cell lysates were immunoprecipitated with anti-FLAG antibodies and immunoblotted with anti-HA antibodies. (J) HEK293T cells were transfected with control, MYC-USP21 WT, or CA mutant for 24 h, and then infected with SeV for the indicated time points. Cell lysates were immunoprecipitated with anti–RIG-I antibodies and immunoblotted with anti-Ub antibodies. Data are representative of two (D–F) or at least three (A–C and G–J) independent experiments.

USP21 binds to and deubiquitinates RIG-I

To examine the targets of USP21 in RIG-I–mediated IRF3 activation, we transfected MYC-USP21 into HEK293T cells along with FLAG-RIG-I-CARD, FLAG-MAVS, or FLAG-TBK1. We found that MYC-USP21 proteins coimmunoprecipitated with FLAG-RIG-I-CARD but not with FLAG-MAVS and FLAG-TBK1 (Fig. 2 A). The binding between MYC-USP21 and FLAG-RIG-I-CARD proteins were also confirmed by immunoprecipitation with anti-FLAG antibodies and immunoblotting with anti-MYC antibodies (unpublished data).

To determine whether the molecular interaction of USP21 and RIG-I is dependent on virus infection, we transfected MYC-USP21 and FLAG-RIG-I plasmids into

HEK293T cells and treated with SeV for indicated time points. MYC-USP21 and FLAG-RIG-I were coimmunoprecipitated regardless of virus infection (Fig. 2 B). To study the physiological function of USP21, we generated rabbit polyclonal antibodies against USP21. Using this antibody, we found that endogenous USP21 coimmunoprecipitated with RIG-I in HeLa cells regardless of SeV infection (Fig. 2 C). Consistently, transfected GFP-USP21 or endogenous USP21 colocalized with transfected FLAG-RIG-I-CARD and endogenous RIG-I regardless of SeV infection (Fig. 2, D–F). These results strongly suggest that USP21 binds to RIG-I.

The Lys63-linked polyubiquitination of RIG-I plays an essential role in virus-induced IRF3 activation (Gack et al., 2007). We reasoned that USP21 might deubiquitinate RIG-I to inhibit virus-induced IRF3 activation. To test this hypothesis, FLAG-RIG-I-CARD and HA-Ub plasmids were co-transfected with control or MYC-USP21 WT or C221A mutant into HEK293T cells. Cell lysates were heated in the presence of 1% SDS and diluted with lysis buffer to disrupt non-covalent protein–protein interactions. Overexpression of USP21 WT but not C221A mutant abrogated FLAG-RIG-I-CARD polyubiquitination (Fig. 2 G). Next, we analyzed the role of USP21 in the deubiquitination of FLAG-RIG-I-CARD in vitro. Because USP21 is unstable when expressed in bacteria (Ye et al., 2011) and is difficult to be purified from prokaryotic system, we immunoprecipitated MYC-USP21 proteins expressed in HEK293T cells with anti-MYC antibodies and then co-incubated MYC-USP21 proteins with cell lysates containing polyubiquitinated FLAG-RIG-I-CARD. The ubiquitination level of FLAG-RIG-I-CARD was significantly decreased by incubation with USP21 WT but not C221A mutant (Fig. 2 H). We further examined the role of USP21 in the inhibition of SeV-induced RIG-I polyubiquitination and found that overexpression of USP21 WT but not C221A mutant inhibited SeV-induced polyubiquitination of both FLAG-tagged and endogenous RIG-I (Fig. 2, I and J). Together, our results demonstrate that USP21 acts as a RIG-I deubiquitinase.

The RLRs family includes three members (RIG-I, MDA5, and LGP2), which have been shown to mediate antiviral response to different stimulators (Kato et al., 2006; Satoh et al., 2010). Interestingly, we found that overexpression of USP21 WT but not C221A mutant inhibited IFN-β, NF-κB, and ISRE reporter activities in HEK293T cells in response to transfected poly(I:C), which was known to be mediated by MDA5 (unpublished data), suggesting that USP21 might also target MDA5. Indeed, overexpression of USP21 WT but not C221A mutant inhibited Lys63-linked polyubiquitination of MDA5 and MDA5-mediated IFN-β, NF-κB, and ISRE reporter activities (unpublished data) and USP21 could also bind to MDA5 and LGP2 (unpublished data). These findings suggest that USP21 also acts as a MDA5 deubiquitinase to inhibit MDA5-mediated antiviral response.

To further understand the functional differences of USP21, CYLD, and A20 in antiviral signaling, we tested their effect on SeV-, RIG-I-CARD–, and TBK1-induced IFN-β, NF-κB, and ISRE reporter activities. We found that the deubiquitinase activity of USP21 was required for its strong inhibitory effect on SeV- and RIG-I-CARD–induced IFN-β, NF-κB, and ISRE reporter activities (unpublished data). Although A20 strongly inhibited SeV- and RIG-I-CARD–induced IFN-β, NF-κB, and ISRE reporter activities, its deubiquitinase activity was not required (unpublished data). Interestingly, the inhibitory effect of CYLD is relatively weaker compared with USP21 and A20 in these assays (unpublished data). However, CYLD strongly inhibited TBK1-induced ISRE reporter activity, whereas USP21 had no obvious effect on TBK1-induced ISRE reporter activity (unpublished data). These results suggest USP21, A20, and CYLD use quite different mechanisms to regulate antiviral signaling.

To further dissect the distinct mechanism of these three deubiquitinases (USP21, A20, and CYLD) in antiviral signaling, we compared their deubiquitinase activities and binding affinities to RIG-I-CARD. CYLD failed to deubiquitinate RIG-I-CARD both in vivo and in vitro (Fig. 3, A and B). Although A20 inhibited RIG-I-CARD polyubiquitination in vivo, it failed to do so in vitro (Fig. 3, A and B). In contrast, USP21 showed a much higher deubiquitinase activity to RIG-I-CARD both in vivo and in vitro (Fig. 3, A and B). Consistently, we found USP21 but not A20 or CYLD coimmunoprecipitated with RIG-I-CARD (Fig. 3 C). Together, these data suggest that USP21 is a bona fide RIG-I deubiquitinase.

USP21 inhibits TRIM25- and RNF135-mediated RIG-I polyubiquitination and activation

Two E3 ligases RNF135 and TRIM25 have been suggested to target RIG-I for Lys63-linked polyubiquitination and are required for antiviral response (Gack et al., 2007; Oshiumi et al., 2010). To uncover whether USP21 affects RNF135- and TRIM25-mediated RIG-I polyubiquitination and activation, we first tested the effect of USP21 on RNF135-mediated RIG-I activation. Overexpression of RNF135 alone could not induce IFN-β reporter activity, whereas once co-overexpressed with RIG-I, RNF135 robustly induced IFN-β reporter activity, which was strongly inhibited by USP21 WT but not C222A mutant (Fig. 4 A and not depicted). Furthermore, USP21 WT but not C221A mutant also strongly inhibited RIG-I and RNF135-induced NF-κB and ISRE reporter activities (unpublished data). For A20, its deubiquitinase activity was not required for its inhibitory effect on RNF135-mediated RIG-I activation (unpublished data). Moreover, USP21 deubiquitinated RNF135-mediated RIG-I polyubiquitination both in vivo and in vitro (Fig. 4, C and D). However, CYLD had no significant effect on RNF135-mediated RIG-I polyubiquitination, whereas A20 inhibited RNF135-mediated RIG-I polyubiquitination in vivo but not in vitro (Fig. 4, C and D).

Consistent with a previous study (Gack et al., 2007), TRIM25 enhanced SeV- and RIG-I–induced IFN-β activity (Fig. 4 B and not depicted). USP21 inhibited TRIM25-mediated IFN-β reporter activities, which was also inhibited by CYLD and A20, but the deubiquitinase activity of A20 was

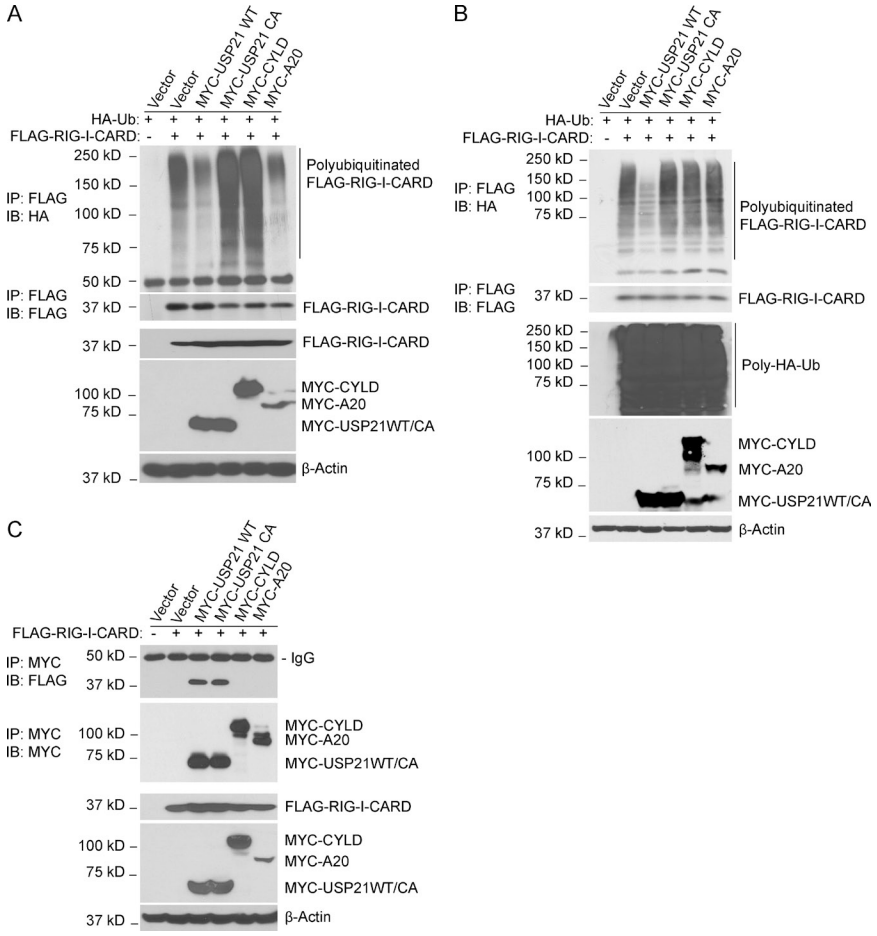

Figure 3. USP21 but not A20 and CYLD binds to and deubiquitinates RIG-I-CARD. (A) FLAG-RIG-I-CARD and HA-Ub were co-transfected with MYC-USP21 WT, CA mutant, MYC-CYLD, or MYC-A20. The heated cell lysates were immunoprecipitated with anti-FLAG antibodies and immunoblotted with anti-HA antibodies. (B) HEK293T cells were transfected with MYC-USP21 WT, CA mutant, MYC-CYLD, or MYC-A20. MYC-tagged proteins were immunoprecipitated with anti-MYC antibodies. Supernatant containing polyubiquitinated FLAG-RIG-I-CARD proteins were co-incubated with the immunoprecipitated MYC-tagged proteins for 2 h at 30°C, and then immunoprecipitated with anti-FLAG antibodies and immunoblotted with anti-HA antibodies. (C) FLAG-RIG-I-CARD was co-transfected into HEK293T cells with control, MYC-USP21 WT, CA mutant, MYC-CYLD, or MYC-A20. Cell lysates were immunoprecipitated with anti-MYC antibodies and immunoblotted with anti-FLAG antibodies. Data from A–C are representative of three independent experiments.

not required (Fig. 4 B and not depicted). These results demonstrate that USP21 inhibits TRIM25- or RNF135-mediated RIG-I polyubiquitination and activation to negatively regulate antiviral signaling.

Generation of USP21 deficient mice

To further study the function of USP21 in antiviral responses, USP21 knockout mice were generated. We constructed the USP21 conditional targeting vector with which the two-*loxP* and two-*frt* strategy was used to obtain homologous recombination in embryonic stem (ES) cells (Fig. 5 A). USP21 heterozygous knockout mice were generated by breeding USP21 conditional knockout mice with Cre transgenic mice to delete USP21 exons 3 and 4, which encode part of essential USP domain (Fig. 5 A). Breeding of USP21 heterozygous male and female mice gave rise to a litter of mice with WT ($^{+/+}$), heterozygous ($^{+/-}$), and homozygous ($^{-/-}$) genotypes with a Mendel ratio, suggesting that USP21$^{-/-}$ mice are viable (Fig. 5 B). RT-PCR and immunoblotting analysis of USP21 expression in MEFs showed that endogenous WT USP21 transcription and protein expression were abolished in USP21$^{-/-}$ mice (Fig. 5, C and D).

USP21$^{-/-}$ mice are viable and fertile. The young USP21$^{-/-}$ mice (4 wk old) showed no gross defects in growth or survival when housed in pathogen-free condition. However, the spleens from 9 wk old USP21$^{-/-}$ mice were significantly larger than the ones from WT littermate controls (Fig. 5, E and F). The total splenocyte number was slightly increased in USP21$^{-/-}$ mice (unpublished data). Flow cytometric analysis of splenocytes revealed an increased percentage of macrophages and neutrophils in USP21$^{-/-}$ mice (Fig. 5, G and H). However, the distribution of DCs, T cells and B cells in spleens were similar between USP21$^{-/-}$ and WT mice (unpublished data). To determine whether USP21$^{-/-}$ hematopoietic cells play an important role in splenomegaly development, we transferred WT or USP21$^{-/-}$ BM cells into SCID mice. Both WT and USP21$^{-/-}$ BM cells successfully repopulated in the recipient mice (Fig. 5 I). Spleens from SCID mice transferred with WT or USP21$^{-/-}$ BM cells were slightly enlarged compared with that from non-transferred mice; however, the sizes of spleens from WT and USP21$^{-/-}$ BM transferred mice were comparable (Fig. 5, J–L). These data suggest that USP21$^{-/-}$ hematopoietic cells are insufficient to cause splenomegaly development under pathogen-free condition. No significant difference was observed between thymuses isolated from USP21$^{-/-}$ and WT littermates (unpublished data).

To determine whether USP21 deficiency in mice affect the basal RIG-I protein level and IFNs production, we examined

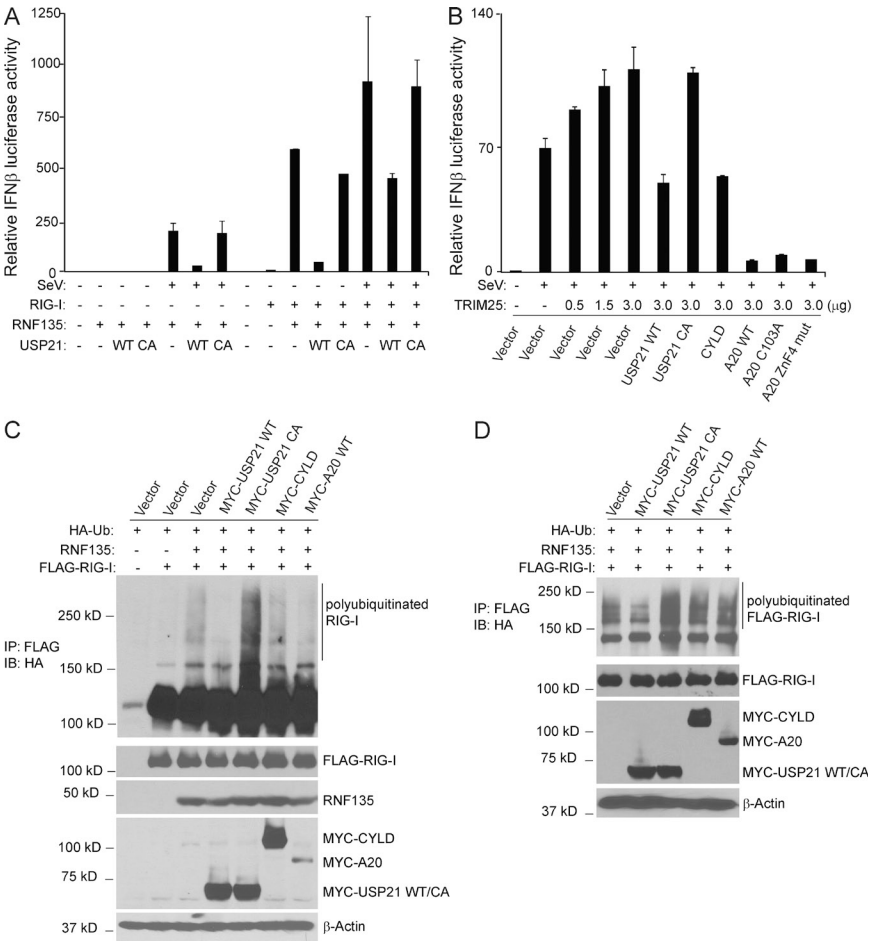

Figure 4. USP21 inhibits TRIM25– and RNF135–induced RIG-I activation. (A) HEK293T cells were transfected with indicated plasmids for 24 h, and then left uninfected or infected with SeV for 12 h before IFN-β luciferase activity was measured. (B) HEK293T cells were transfected with MYC-USP21 WT, CA mutant, MYC-CYLD, or MYC-A20 along TRIM25. Transfected cells were left uninfected or infected with SeV for 12 h before IFN-β luciferase activity was measured. (C) Expression vector encoding FLAG-RIG-I, RNF135, and HA-Ub were co-transfected with control, MYC-USP21 WT, CA mutant, MYC-CYLD, or MYC-A20. Cell lysates were immunoprecipitated with anti-FLAG antibodies and immunoblotted with anti-HA antibodies. (D) HEK293T cells were transfected with expression vectors encoding MYC-USP21 WT, CA mutant, MYC-CYLD, or MYC-A20. MYC-tagged proteins were immunoprecipitated with anti-MYC antibodies. In the parallel experiments, HEK293T cells were transfected with FLAG-RIG-I, RNF135, and HA-Ub. Supernatant containing polyubiquitinated FLAG-RIG-I proteins were incubated with immunoprecipitated MYC-USP21 WT, CA mutant, MYC-CYLD, or MYC-A20 for 2 h at 30°C, and then immunoprecipitated with anti-FLAG antibodies and immunoblotted with anti-HA antibodies. Error bars indicate ±SD in duplicate experiments. Data are representative of two (A and B) or three (C and D) independent experiments.

RIG-I protein level in multiple organs and no significant difference was found between 9-wk-old WT and USP21$^{-/-}$ mice (Fig. 5 O). The basal RIG-I protein level in BMDCs and PMs was also comparable between WT and USP21$^{-/-}$ mice (Fig. 5 M). Basal IFN-α/β production in 9-wk-old USP21$^{-/-}$ mice is similar to that in WT mice (Fig. 5 N). Our results suggested that deletion of USP21 in mice did not affect the basal RIG-I expression and IFNs production in 9-wk-old USP21$^{-/-}$ mice with noticeable splenomegaly.

Deletion of USP21 enhances antiviral response in multiple cell types

To further assess the physiological function of USP21, we isolated MEFs from WT and USP21$^{-/-}$ embryos. SeV infection, transfection of poly(I:C), and RIG-I-CARD overexpression resulted in higher IFN-β and ISRE reporter activities in USP21$^{-/-}$ MEFs compared with that in WT MEFs (Fig. 6 A). Consistently, virus-induced IFN-α and -β expressions were much higher in USP21$^{-/-}$ MEFs compared with WT MEFs (Fig. 6 B). Upon infection with VSV-eGFP, USP21$^{-/-}$ MEFs showed significantly decreased number of VSV-eGFP^{+} cells (Fig. 6 C). USP21$^{-/-}$ MEFs were also more resistant to VSV infection compared with WT MEFs (Fig. 6 D). Consistent with these results, VSV and SeV induced a stronger IRF3 phosphorylation in USP21$^{-/-}$ MEFs compared with that in WT MEFs (Fig. 6 E). SeV also induced a stronger IKKα/β phosphorylation in USP21$^{-/-}$ MEFs compared with that in WT MEFs (Fig. 6 E). Furthermore, SeV replication was significantly inhibited in USP21$^{-/-}$ MEFs (Fig. 6 F). Consistently, endogenous USP21 and RIG-I coimmunoprecipitated in MEFs (Fig. 6 G) and SeV induced a stronger RIG-I polyubiquitination in USP21$^{-/-}$ MEFs compared with that in WT MEFs (Fig. 6 H).

Furthermore, SeV induced a stronger IRF3 phosphorylation in USP21$^{-/-}$ PMs compared with that in WT PMs (Fig. 7 A). SeV induced much more IFN-α/β production in USP21$^{-/-}$ PMs compared with that in WT PMs (Fig. 7, B and C). SeV also induced a stronger IRF3 phosphorylation and much more IFN-α/β productions in USP21$^{-/-}$ BMDCs compared with that in WT BMDCs (Fig. 7, D–F). However, we could not observe any significant effect of USP21 deficiency on SeV-induced IRF3 phosphorylation, IFN-α/β production in BM-derived macrophages (BMMs; unpublished data). It is noteworthy that USP21 expression level was much lower in BMMs compared with MEFs, BMDCs, and PMs (unpublished data).

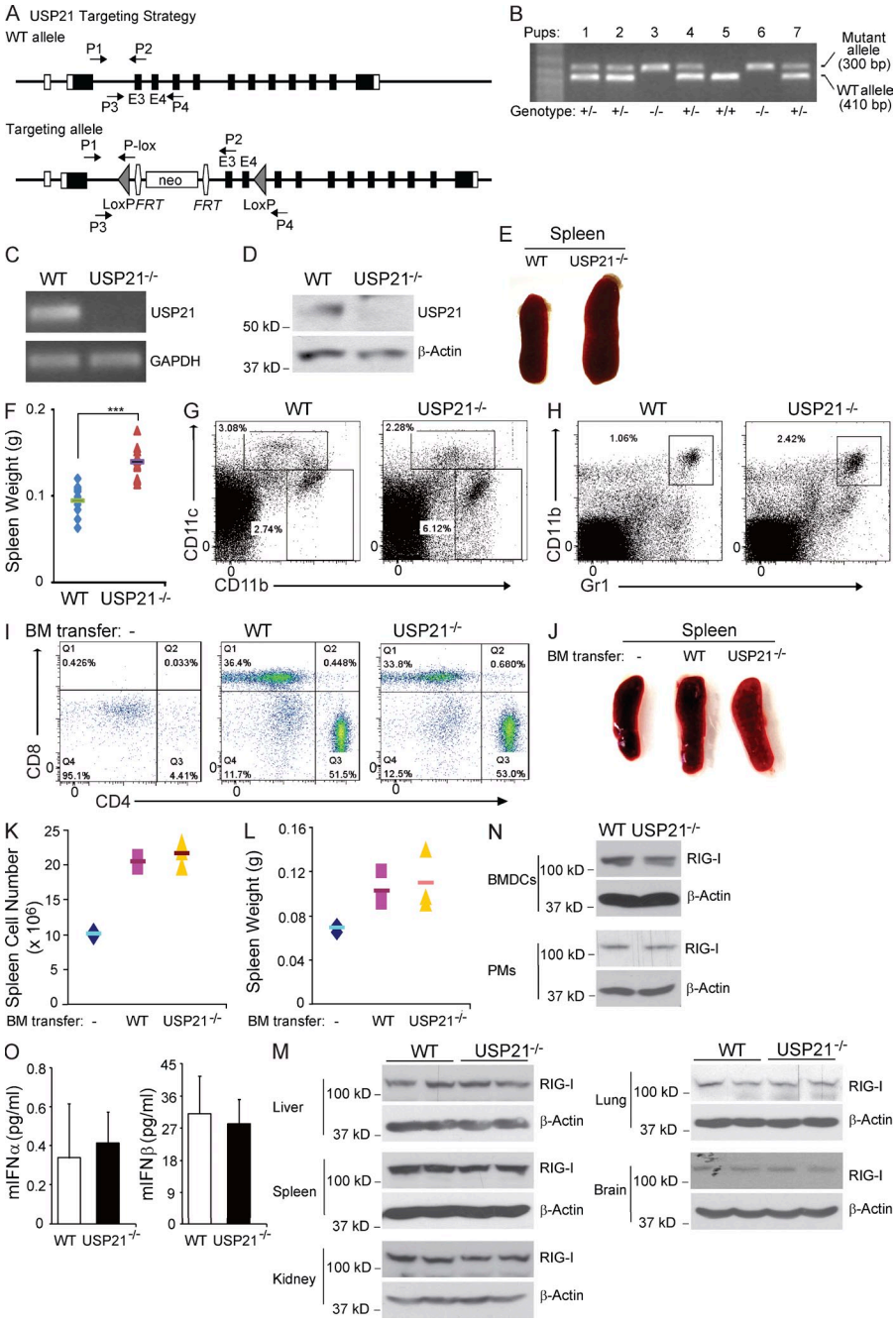

Figure 5. Generation of USP21 knockout mice. (A) Generation of USP21 conditional knockout mice by two-*loxP*, two-*frt* strategy. (B) PCR genotyping of WT and USP21$^{-/-}$ littermates generated from USP21$^{+/-}$ mice intercrossing. (C) Total RNA was extracted from MEFs and mRNA level of USP21 was examined by RT-PCR. (D) Cell lysates from WT and USP21$^{-/-}$ MEFs were immunoblotted by anti-USP21 antibodies. (E) Representative images of spleens isolated from 9-wk WT and USP21$^{-/-}$ mice. (F) Quantitative analysis of the weight of spleens isolated from 9-wk-old WT (n = 10) and USP21$^{-/-}$ (n = 10) mice. (G) Macrophage and dendritic cell populations in splenocytes from USP21$^{-/-}$ and WT mice were analyzed by FACS using anti-CD11b and anti-CD11c antibodies. (H) Neutrophil populations in splenocytes from USP21$^{-/-}$ and WT mice were analyzed by FACS using anti-Gr1 and anti-CD11b antibodies. (I) SCID mice were transferred with WT or USP21$^{-/-}$ BM cells for 10 wk. T cell populations in splenocytes were analyzed by FACS using anti-mouse CD3, CD4, and CD8 antibodies. (J) Representative images of spleens from naive and BM-transferred SCID mice. (K) Spleens from naive and BM transferred SCID mice were homogenized. Total splenocytes were quantitatively analyzed. (L) Quantitative analysis of the weight of spleens isolated from naive and BM-transferred SCID mice. (M) Fresh BM cells were cultured in the medium with IL-4 and GM-CSF cytokines for 7 d. Cell lysates from BMDCs or PMs were immunoblotted by anti–RIG-I antibodies. (N) Blood was collected from 9-wk-old WT or USP21$^{-/-}$ mice, and IFN level in sera was measured by ELISA kit. (O) Cells from different organs were lysed and immunoblotted by anti–RIG-I antibodies. Error bars indicate ±SD in duplicate experiments. ***, $P < 0.001$ (two-tailed paired Student's t test). Data are representative of two (E–O) or at least three (B–D) independent experiments.

USP21 inhibits antiviral response independent of A20 ubiquitin editing complex

Because A20 has been suggested to negatively regulate antiviral response (Lin et al., 2006; Parvatiyar et al., 2010; Saitoh et al., 2005; Wang et al., 2004), we next determined whether the inhibitory function of USP21 is dependent on A20 ubiquitin-editing complex. USP21 inhibited SeV-induced IFN-β reporter activity in WT, A20$^{-/-}$, ITCH$^{-/-}$, and TAXBP1$^{-/-}$ MEFs (Fig. 8, A–D). USP21 also inhibited RIG-I-CARD–induced IFN-β reporter activity in WT, A20$^{-/-}$, ITCH$^{-/-}$, and TAXBP1$^{-/-}$ MEFs (unpublished data). These results indicate that USP21 function in antiviral response is independent of A20 ubiquitin-editing complex. Next, we examined whether USP21 and A20 can cooperatively inhibit antiviral signaling. Both USP21 and A20 inhibited SeV- and RIG-I-CARD–induced IFN-β reporter activity in a dose-dependent manner. The inhibitory effect of co-overexpression of USP21 and A20 was much stronger than individual expression of USP21 or A20 (Fig. 8 E and not depicted).

Recently, A20 has been suggested to inhibit TNF-induced NF-κB activation by promoting Ubc13 and UbcH5C degradation or disrupting Ubc13 or UbcH5C binding with E3

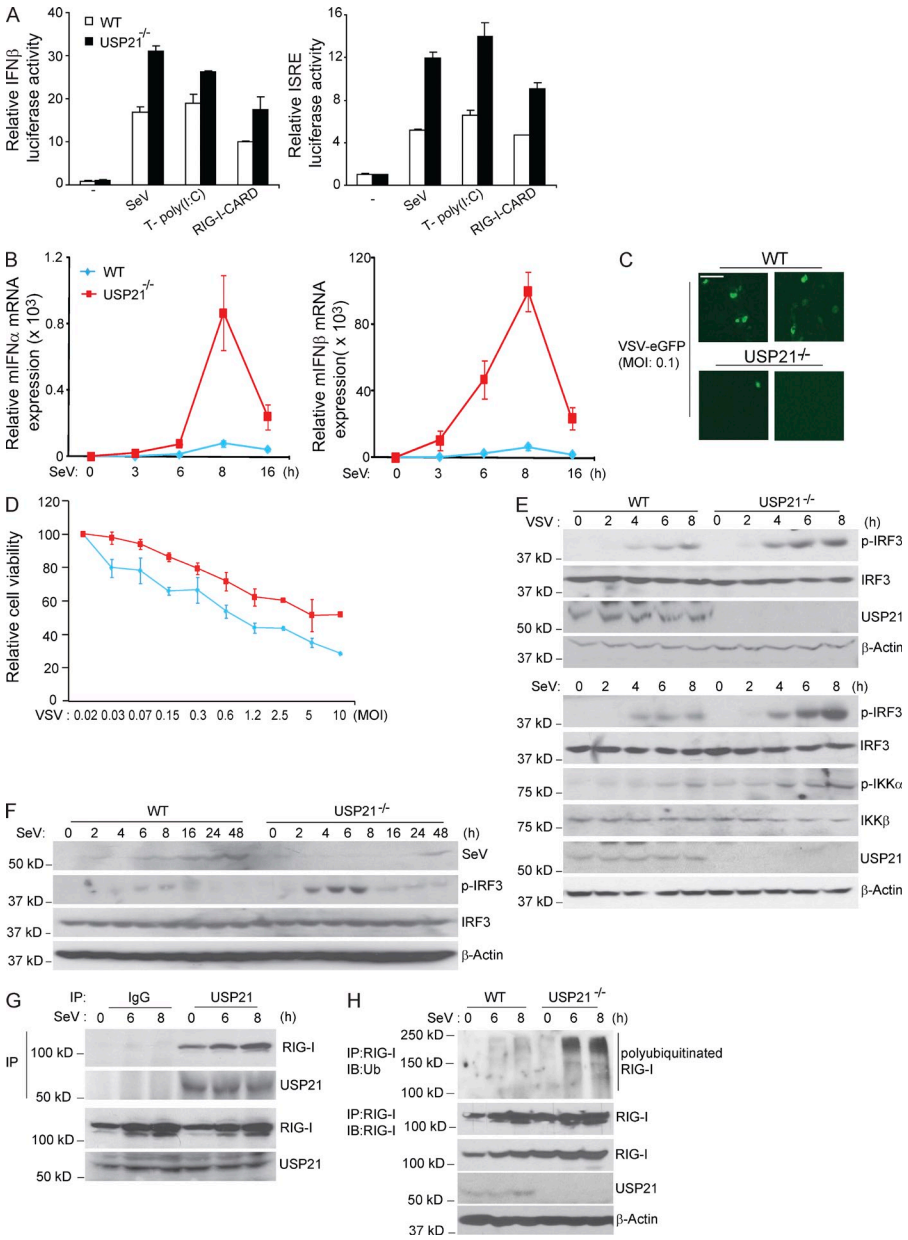

Figure 6. Knockout of USP21 expression enhances antiviral response in MEFs. (A) WT and USP21$^{-/-}$ MEFs were transfected with IFN-β or ISRE reporter along with or without RIG-I-CARD for 24 h, and then left uninfected or infected with SeV or transfected with poly (I:C) for 12 h before luciferase activity was measured. (B) MEFs were treated with SeV for the indicated time points. The mRNA levels of IFN-α/β were measured by real-time RT-PCR. (C) MEFs were infected with VSV-eGFP (moi = 0.1) for 48 h and GFP$^+$ cells were imaged. Bar, 50 µm. (D) MEFs were infected with VSV for the indicated MOI for 48 h and relative cell viability was measured by CCK8 kit. (E) MEFs were infected with VSV or SeV for the time points indicated. Cell lysates were immunoblotted by anti-p-IRF3, anti-IRF3, anti-USP21, anti–p-IKKα/β, anti-IKKβ, and anti–β-actin antibodies. (F) MEFs were infected with SeV for the indicated time points. Cell lysates were immunoblotted by anti-SeV antibodies. (G) MEFs were infected with SeV for the indicated time points. Endogenous USP21 were immunoprecipitated with anti-USP21 antibodies and immunoblotted with anti–RIG-I antibodies. (H) MEFs were infected with SeV for the indicated time points. RIG-I proteins in the cell lysates were immunoprecipitated with anti–RIG-I antibodies and immunoblotted with anti-Ub antibodies. Error bars indicate ±SD in duplicate experiments. Data are representative of two (B–D and F) or three (A, E, G, and H) independent experiments.

ligase (Shembade et al., 2010). Thus, we examined whether A20 inhibits antiviral response via the aforementioned mechanism. Overexpression of USP21, CYLD, and A20 failed to promote Ubc13 and UbcH5C degradation regardless of SeV treatment (unpublished data). Consistently, no significant difference was found in terms of UbcH5C degradation in response to SeV infection in WT, USP21$^{-/-}$, and A20$^{-/-}$ MEFs in the time course examined (unpublished data).

The fact that SeV induced weaker IFN-β reporter activity in A20$^{-/-}$ MEFs compared with WT, ITCH$^{-/-}$, and TAXBP1$^{-/-}$ MEFs suggests that the role of A20 in antiviral response is far to be fully understood (Fig. 8, A–D). To better understand the role of A20 in antiviral response, we infected WT and A20$^{-/-}$ MEFs with SeV and examined the effect of A20 deficiency on SeV-induced IRF3 phosphorylation. Surprisingly, SeV failed to induce IRF3 phosphorylation at earlier time points in A20$^{-/-}$ MEFs (Fig. 8 F). However, at later time points, we did see a weak induction of IRF3 phosphorylation (unpublished data). To further confirm the result, we tested the sensitivity of WT and A20$^{-/-}$ MEF to VSV infection and found that A20$^{-/-}$ MEFs were more sensitive compared with WT MEFs (unpublished data). Consistently, SeV failed to induce IFN-α/β production in A20$^{-/-}$ MEFs (Fig. 8 G and not depicted), although IL-6 expression was comparably induced in both USP21$^{-/-}$ and A20$^{-/-}$ MEFs (unpublished data). These results indicate that the physiological role of A20 in antiviral response is very complicated and its function in antiviral response needs to be further investigated.

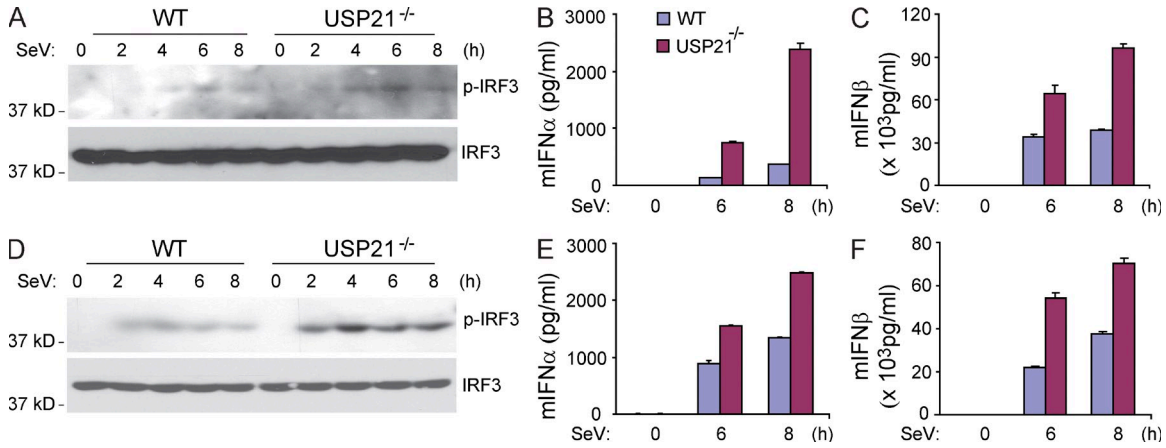

Figure 7. Knockout of USP21 expression enhances antiviral response in PMs and BMDCs. (A) PMs isolated from WT and USP21$^{-/-}$ mice were infected by SeV with the indicated time points. Cell lysates were immunoblotted by anti-p-IRF3 and anti-IRF3 antibodies. (B and C) PMs were infected by SeV with the indicated time points. IFN-α (B) and IFN-β (C) production in cell culture medium were measured by ELISA kit. (D) BMDCs were infected by SeV with the indicated time points. Cell lysates were immunoblotted by anti-p-IRF3 and anti-IRF3 antibodies. (E and F) BMDCs were infected by SeV with the indicated time points. IFN-α (E) and IFN-β (F) production in cell culture medium was measured by ELISA kit. Error bars indicate ±SD in duplicate experiments. Data from A–F are representatives of two independent experiments.

Deletion of USP21 enhances antiviral immune defense in vivo

To investigate the role of USP21 in vivo, WT and USP21$^{-/-}$ mice were injected with VSV through tail vein, and then sera were collected to measure type-I IFN level. We found that tail vein injection of VSV induced a stronger production of IFNs in USP21$^{-/-}$ mice compared with that in WT mice, whereas the steady-state levels of IFNs without VSV infection were similarly very low in both WT and USP21$^{-/-}$ mice (Fig. 9, A and B). Consistently, the viral titers in sera were much lower in USP21$^{-/-}$ mice than those in WT mice at all time points examined (Fig. 9 C). USP21 deficiency did not affect VSV entry into the MEFs and mice organs (unpublished data). These results suggest that USP21 deficiency enhances viral clearance caused by a higher level of type-I IFN induction.

To determine whether USP21 deficiency affects the survival of mice after VSV infection, mice were infected with VSV through tail vein and their survival was monitored. We found that USP21$^{-/-}$ mice were more resistant to VSV-induced lethality (Fig. 9 D). At day 8 after infection, ∼40% of WT mice died, whereas no USP21$^{-/-}$ mice died until day 10. After 2 wk of VSV infection, splenomegaly in USP21$^{-/-}$ mice was even more severe than that in naive mice (Fig. 9, E and F). SCID mice transferred with USP21$^{-/-}$ BM cells developed splenomegaly after VSV infection and were resistant to VSV-induced lethality (Fig. 9, G-I). These results suggest that USP21$^{-/-}$ hematopoietic cells are sufficient to cause splenomegaly development in mice infected with VSV and protect mice from VSV-induced lethality.

Consistent with the results obtained by intravenous VSV infection, intraperitoneal injection of VSV also induced a stronger production of IFNs in USP21$^{-/-}$ mice compared with that in WT mice (Fig. 9, J and K). Virus titer detected in different organs of USP21$^{-/-}$ mice was significantly lower compared with that in WT mice (Fig. 9 L). 4-wk-old USP21$^{-/-}$ mice did not show noticeable splenomegaly and basal RIG-I expression in 4-wk old WT and USP21$^{-/-}$ mice was comparable (unpublished data). Intraperitoneal injection of VSV in 4-wk-old USP21$^{-/-}$ also induced a stronger IFN production compared with that in 4-wk-old WT mice (unpublished data). Collectively, our data indicate that USP21 negatively regulates antiviral response in vivo and the hyper-responsiveness of USP21-deficient mice to VSV is not due to splenomegaly or increased basal RIG-I expression.

DISCUSSION

Excessive production of IFNs or proinflammatory cytokines is destructive to hosts, thus a successful immune response against viral infections must be tightly regulated. Lys63-linked polyubiquitination of RIG-I is a pivotal event in RIG-I–mediated antiviral response. USP21 is a highly conserved deubiquitinase and its physiological role is largely unknown. Biochemical study and crystal structure showed that USP21 is a highly active deubiquitinating enzyme that can efficiently cleave Lys63-linked ubiquitin chain (Nakagawa et al., 2008; Xu et al., 2010; Ye et al., 2011; García-Santisteban et al., 2012; Urbé et al., 2012). In this study, we present biochemical and genetic evidences that USP21 acts as a RIG-I deubiquitinase to negatively regulate RIG-I–mediated antiviral signaling through its deubiquitinase activity. The inhibitory effect of USP21 on antiviral signaling is independent of A20 ubiquitin-editing complex. USP21 inhibits RNA virus-induced Lys63-linked polyubiquitination of RIG-I and RIG-I–mediated downstream signaling. Genetic deletion of USP21 gene in mice enhances RIG-I–mediated antiviral response. Furthermore, we also found that USP21 binds to two other RLR family members (MDA5 and LGP2) and deubiquitinates MDA5, suggesting USP21 acts as a major negative regulator

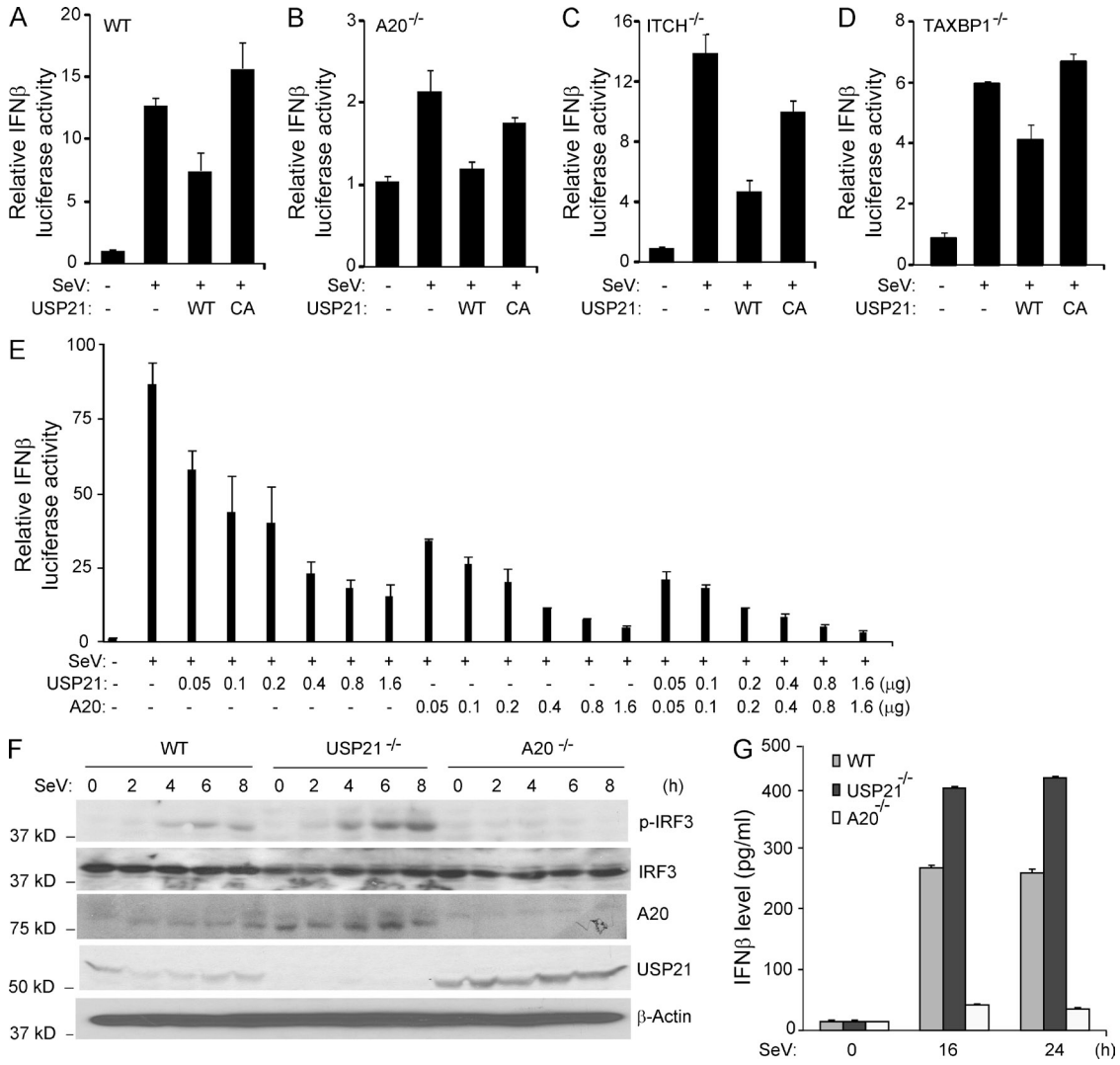

Figure 8. USP21 negatively regulates antiviral response independent of A20 ubiquitin-editing complex. (A–D) WT, A20$^{-/-}$, ITCH$^{-/-}$, and TAXBP1$^{-/-}$ MEFs were transfected with IFN-β reporter along with MYC-USP21 WT or CA mutant for 24 h, and then left uninfected or infected with SeV for 12 h before luciferase activity was measured. (E) HEK293T cells were transfected with the indicated plasmids along with IFN-β luciferase reporter for 24 h, and then infected with SeV or left untreated for 12 h before luciferase assays were performed. (F) WT, USP21$^{-/-}$, and A20$^{-/-}$ MEFs were infected with SeV with the indicated time points. Cell lysates were immunoblotted by the indicated antibodies. (G) WT, USP21$^{-/-}$, and A20$^{-/-}$ MEFs were infected with SeV with the indicated time points. IFN-β production was determined by ELISA kit. Error bars indicate ±SD in duplicate experiments. The data from A–G are representative of two independent experiments.

to restrict RLR-mediated antiviral responses through deubiquitinating RIG-I and MDA5.

Ubiquitin can be covalently attached to other proteins through a stepwise enzymatic reaction involving three classes of enzymes (E1, E2, and E3). In addition, ubiquitination can be reversed by DUBs that comprise a large family of proteins (Nijman et al., 2005). Both ubiquitination and deubiquitination play regulatory roles in a broad spectrum of cellular processes, including immune response (Bhoj and Chen, 2009; Wertz and Dixit, 2010). In the process of ubiquitination and deubiquitination, E3 ligases and DUBs recognize the substrates and primarily determine the substrate specificity, which attract much effort for identification of substrate-specific E3 ligases and DUBs. Two E3 ligases, TRIM25 and RNF135, have been reported to catalyze Lys63-linked polyubiquitination of RIG-I and are essential for antiviral response (Gack et al., 2007, 2008; Oshiumi et al., 2009, 2010). However, the molecular mechanisms of TRIM25 and RNF135 function in antiviral signaling are different. Unlike TRIM25, RNF135 alone is sufficient to polyubiquitinate and activate RIG-I (Fig. 4 and not depicted). It has been shown that TRIM25 and RNF135 catalyze RIG-I polyubiquitination on different domains (Gack et al., 2007; Oshiumi et al., 2009). Interestingly, USP21 inhibits both TRIM25- and RNF135-mediated antiviral response and RIG-I activation (Fig. 4 and not depicted). Therefore, it is highly likely that USP21 acts

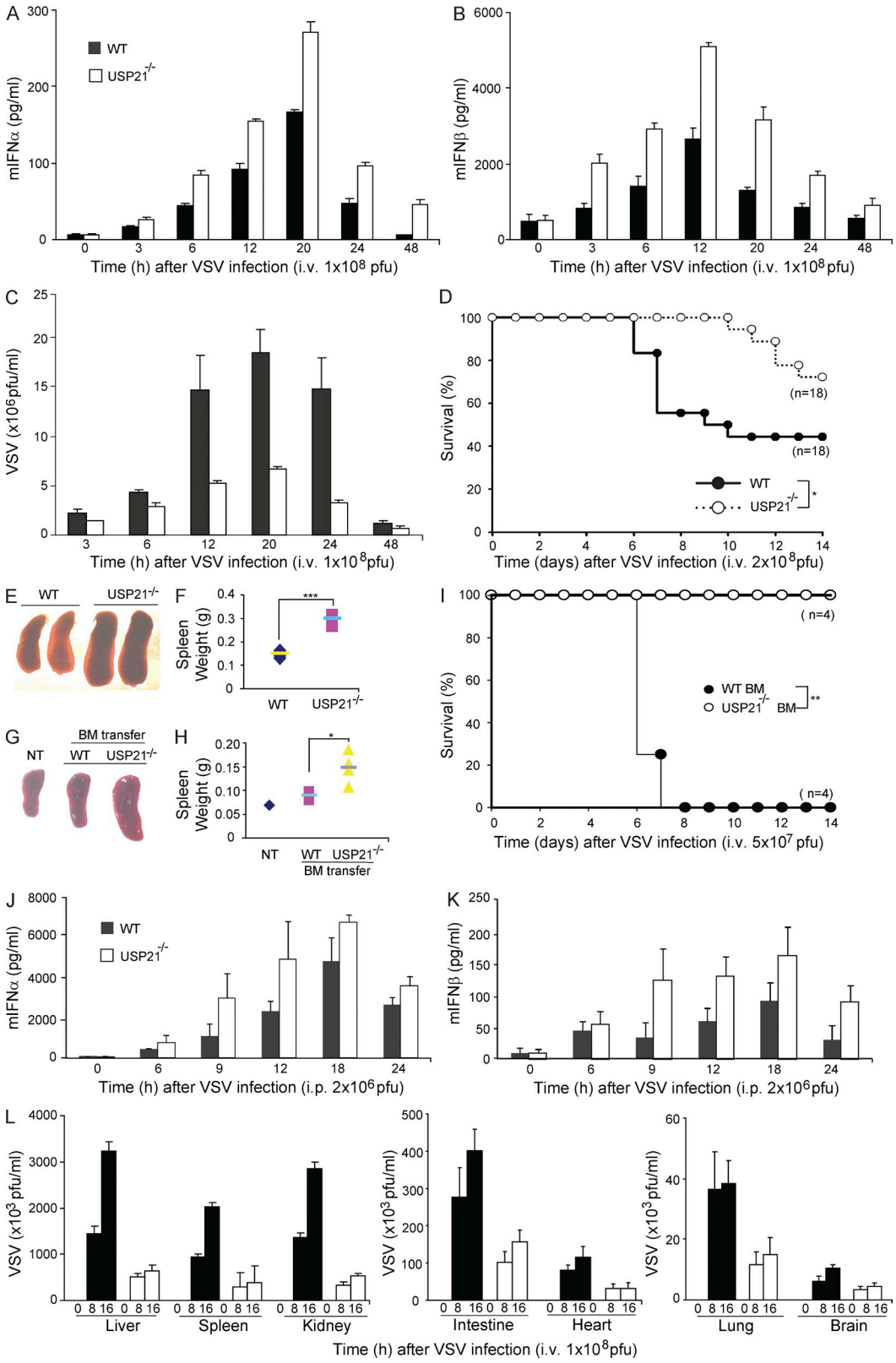

Figure 9. Knockout of USP21 expression enhances antiviral response in vivo. (A and B) WT and USP21$^{-/-}$ mice were injected with VSV (1 × 10^8 pfu) via tail vein for the indicated time period. Amounts of IFN-α and IFN-β in sera were measured by ELISA. (C) WT and USP21$^{-/-}$ mice were infected with VSV (1 × 10^8 pfu) via tail vein injection. Sera collected at the indicated time points were used for measurement of viral titers by plaque assays. (D) WT (n = 18) and USP21$^{-/-}$ (n = 18) mice were infected with VSV (2 × 10^8 pfu) via tail vein injection and the survival of the mice was monitored for 2 wk.

as a RIG-I polyubiquitination guard to prevent extensive RIG-I polyubiquitination.

A20 contains one N-terminal deubiquitinase domain and seven C-terminal zinc-finger (ZnF) domains, and it plays a key role in the negative regulation of inflammation and immunity. A20 has been shown to turn off TNF-induced NF-κB activation by modulating both Lys48- and Lys63-linked polyubiquitin chains (Wertz et al., 2004). Induction of Lys48 polyubiquitination by A20 requires its C-terminal ZnFs ubiquitin-binding domain, which may promote interaction with E3 ligases (Itch and RNF11; Shembade et al., 2007, 2008, 2009). A20 is thought to promote deubiquitination of Lys63-linked polyubiquitin chains either directly through its N-terminal deubiquitinase domain or by disrupting the interaction between E3 and E2 enzymes (Shembade et al., 2010). Interestingly, in our in vitro assay, USP21 deubiquitinates RIG-I-CARD, whereas A20 fails to do so, even though both USP21 and A20 inhibit RIG-I-CARD overexpression-induced RIG-I-CARD polyubiquitination in vivo (Fig. 3). Furthermore, polyubiquitinated RIG-I mediated by RNF135 can be deubiquitinated by USP21 but not A20 in vitro even though both USP21 and A20 inhibit RNF135-induced RIG-I polyubiquitination in vivo (Fig. 4). In addition, RIG-I-CARD co-immunoprecipitates with USP21 but not with A20 (Fig. 3 C). These results suggest that A20 blocks the polyubiquitination of RIG-I in vivo not by acting as a direct RIG-I deubiquitinase.

Ubc13 and UbcH5C play essential roles in TNF-induced NF-κB activation and RIG-I–mediated antiviral signaling (Xia et al., 2009; Yamazaki et al., 2009; Zeng et al., 2009; Zeng et al., 2010). In TNF-induced signaling, A20 inhibits TNF-induced NF-κB activation by promoting Ubc13 and UbcH5C degradation (Shembade et al., 2010). However, unlike in TNF signaling, SeV fails to induce Ubc13 and UbcH5C degradation in the tested time courses (unpublished data). Surprisingly, opposite to overexpression data, SeV fails to induce antiviral response at the earlier time course in $A20^{-/-}$ MEFs and $A20^{-/-}$ MEFs are more sensitive to VSV-induced cell death compared with WT MEF (Fig. 8 and not depicted). Therefore, the physiological role of A20 in antiviral response is more complicated than what we have expected from A20 overexpression data. It may both positively and negatively regulate antiviral response and its function in antiviral signaling may be determined by its protein level in cells. At the low protein level, A20 may be essential for antiviral response, whereas at the high protein level, it may inhibit antiviral response. However, the precise molecular mechanism of A20 in antiviral response remains to be further determined.

Another deubiquitinase, CYLD, has been suggested to deubiquitinate RIG-I (Friedman et al., 2008; Zhang et al., 2008). CYLD also binds to TBK1 and $CYLD^{-/-}$ DCs show constitutive activation of TBK1 (Friedman et al., 2008; Zhang et al., 2008). Consistent with these previous studies, CYLD strongly inhibits TBK1-induced ISRE reporter activity (unpublished data). However, CYLD fails to inhibit and deubiquitinate RIG-I-CARD overexpression-induced RIG-CARD polyubiquitination both in vivo and in vitro (Fig. 3). Together, these results suggest that CYLD targets TBK1 or its downstream molecules to negatively regulate antiviral response. More interestingly, a recent study showed loss of CYLD renders mice considerably more susceptible to VSV infection (Zhang et al., 2011). Therefore, the physiological role and the true targets of CYLD in antiviral response need to be further investigated.

$USP21^{-/-}$ mice develop splenomegaly and have an increased percentage of macrophages in spleen. USP21 negatively regulates antiviral responses in PMs and BMDCs. However, we did not observe any significant effect of USP21 deficiency on antiviral response in BMMs in vitro. It is noteworthy that USP21 expression level is much lower in BMMs compared with that in MEFs, BMDCs, and PMs (unpublished data). It is very likely that USP21 expression is suppressed in the BMMs under in vitro culture condition. Although $USP21^{-/-}$ hematopoietic cells are insufficient to cause splenomegaly development under pathogen-free conditions, they are sufficient to cause splenomegaly development in recipient mice infected with VSV and to protect mice from VSV-induced lethality. These results strongly suggest that hematopoietic cells contribute significantly to USP21-mediated negative regulation of antiviral response.

Deubiquitination is a common mechanism used by hosts to tightly regulate the antiviral response. In addition to USP21, A20, and CYLD, DUBA has been shown to down-regulate antiviral signaling by deubiquitinating TRAF3 (Kayagaki et al., 2007). To our knowledge, only few deubiquitinases have been studied in knockout mouse model to explore their physiological functions in different biological processes, especially in antiviral response. USP21 is unique because its deubiquitinase activity is required for its function and USP21-deficient mice spontaneously develop splenomegaly and are resistant to VSV infection.

(E) Representative images of spleens isolated from WT and $USP21^{-/-}$ mice 2 wk after intravenous VSV (2×10^8 pfu) infection. (F) Quantitative analysis of the weight of spleens isolated from 9-wk-old WT ($n = 5$) and $USP21^{-/-}$ ($n = 5$) mice 2 wk after intravenous VSV (2×10^8 pfu) infection. (G and H) SCID mice were transferred with WT and $USP21^{-/-}$ BM cells and infected with VSV (1×10^7 pfu) for 2 wk. Representative spleens (G) were shown and spleen weight (H) was measured. (I) SCID mice transferred with WT and $USP21^{-/-}$ BM cells were infected with VSV (5×10^7 pfu) via tail vein injection and the survival of the mice was monitored for 2 wk. (J and K) WT and $USP21^{-/-}$ mice were injected intraperitoneally with VSV (2×10^6 pfu) for the indicated time courses. Amount of IFN-α (J) and IFN-β (K) in sera was measured by ELISA. (L) WT and $USP21^{-/-}$ mice were injected with VSV (1×10^8 pfu) through tail vein for the indicated time points. Mice were sacrificed and viral titers in organs were determined by the plaque assay. Error bars indicate ±SD in duplicate experiments. *, $P < 0.05$; **, $P < 0.01$; ***, $P < 0.001$ (two-tailed paired Student's *t* test or Kaplan Meier survival analysis). Data are representative of two (A–C and E–L) or at least three (D) independent experiments.

Inhibition of USP21 deubiquitinase activity may enhance antiviral response and could be beneficial to certain patients with low immune activity.

MATERIALS AND METHODS

Generation of USP21-deficient mice. We constructed the USP21-conditional targeting vector with which the two-*loxP* and two-*frt* strategy was used to delete the exon 3 and 4 that encodes part of essential USP21 USP domain. Homologous recombination in mouse ES cells and blastocyst injection of ES cells were performed at the Baylor College of Medicine core facility. $USP21^{+/flox\text{-}frt\text{-}neo}$ mice were crossed with Meox2-Cre mice to generate $USP21^{+/-}$ mice with deletion of exon 3 and 4, and reading frame shift was mediated by loxP-mediated DNA recombination. $USP21^{+/-}$ mice were intercrossed to generate $USP21^{-/-}$ and WT littermates. $USP21^{-/-}$ mice were backcrossed for five generations to the C57BL/6 background. Age-matched WT and $USP21^{-/-}$ littermates were used for all experiments. The following primers were used for genotyping mouse USP21 allele: P1, 5′-AGAATTCTTCCTTGGGTCCT-3′; P2, 5′-GTCATCCTACCTCACTGGTC-3′; P-LOX, 5′-AGGTGGATCCATCATATGAGA-3′; P3, 5′-CTAGGCTGCTTGCAGTTGGA-3′; P4, 5′-GTGGCTAGAAAATCTCTAGG-3′. The following primers were used for genotyping Cre transgenic allele: CreMice-COM-5, 5′-GGGACCACCTTCTTTTGGCTTC-3′; CreMice-WT-3, 5′-AAGATGTGGAGAGTTCGGGGTAG-3′; CreMice-MUT-3, 5′-CCAGATCCTCCTCAGAAATCAGC-3′. The following primers were used for RT-PCR analysis of USP21 expression: mUSP21-RT-5, 5′-GCTCACCACACACTGCTTCT-3′; mUSP21-RT-3, 5′-GGATTCACAGCTTCACAGGA-3′. All animal experiments were performed in accordance with protocols approved by the Institutional Animal Care and Use Committee of Baylor College of Medicine.

BM reconstitution in SCID mice. The Rag1/severe complex immune deficiency (SCID) mice (The Jackson Laboratory), ages 8–12 wk, were bred and maintained in a specific pathogen–free animal facility. BM cells from ∼8-wk-old WT and $USP21^{-/-}$ mice were isolated from femoral bones. A total of 50 million BM cells per mouse were intravenously injected into lethally irradiated (500 cGy) 10-wk-old SCID mice. Success of transplantation was confirmed by flow cytometry analysis using PE-labeled anti-CD4 and APC-Cy7–labeled anti-CD8 antibodies after 10 wk of transplantation. BM chimeras were further infected with VSV at different doses. Spleens from these chimeras were analyzed 10 wk after transplantation.

Isolation of MEFs, PMs, BMDCs, and BMMs. WT and $USP21^{-/-}$ MEFs were prepared from day 13.5 embryos and cultured in DMEM supplemented with 10% FBS. $A20^{-/-}$, $TAXBP1^{-/-}$, and $ITCH^{-/-}$ MEFs were provided by A. Ma (University of California, San Francisco, CA), E.W. Harhaj (Johns Hopkins School of Medicine, Baltimore, MD), and L. Matesic (University of South Carolina, Columbia, SC), respectively. PMs were harvested by flushing peritoneal cavities from 8-wk-old mice. BMDCs and BMMs were generated by flushing BM cells from femurs and tibiae of mice. Cells were cultured in M-CSF or GM-CSF/IL-4 conditional media for 7 d to generate BMMs and BMDCs respectively.

Reagents and antibodies. Mouse monoclonal antibodies against MYC (sc-40), HA (sc-7392), and Ub (sc-8017), rabbit polyclonal antibodies against RNF135 (sc-102092) and IRF3 (sc-9082), and protein A–agarose were from Santa Cruz. Mouse monoclonal antibodies against β-actin (A2228) and FLAG (F3165) were from Sigma-Aldrich. Rabbit monoclonal antibodies against RIG-I (3743) and p-IRF3 (4947), rabbit antibodies against phospho-IKKα/β (2078S), and IKKβ (2684S) were obtained from Cell Signaling Technology. Mouse monoclonal antibodies against RIG-I (ALX-804-849) were purchased from Enzo Life Science. Anti-Sendai virus (PD029) antibodies were obtained from Medical and Biological Laboratories. Texas Red–labeled anti–mouse antibodies (T862), Oregon Green labeled anti–rabbit antibodies (P36930), and anti-Ubc13 antibodies (371100) were purchased from Invitrogen. Anti-UbcH5C antibodies (ab106315) were obtained from Abcam. Anti–mouse CD16/32 (101301) antibodies were obtained from BioLegend. Pacific Blue–labeled anti-CD3 (558214), APC-Cy7–labeled anti-CD8 (561967), PE-labeled anti-CD4 (553652), APC-labeled anti–Gr-1 (561083), PerCP-Cy5.5–labeled anti-CD11b (561114), PE-labeled anti-CD11c (561044), APC-labeled anti-B220 (561880), FITC-labeled anti-CD21/35 (561769), and PE-labeled anti-IgM (562033) were purchased from BD. Anti-USP21 antibodies were generated by immunizing rabbits with the synthetic peptides corresponding to amino acids MPQASEHRLGRTREPP, RLALRPEPPTLRRSTSLR, NAPVCDRCRQKTRSTKKLTV (Genemed Synthesis, Inc.). Cell culture medium was obtained from Invitrogen. Nitrocellulose membrane was purchased from Bio-Rad.

Constructs. The NF-κB–dependent firefly luciferase reporter plasmid and pCMV promoter-dependent *Renilla* luciferase reporter plasmids were purchased from Takara Bio Inc. ISRE luciferase reporter plasmid was provided by R. Wang (The Methodist Hospital Research Institute, Houston, TX). IFN-β luciferase reporter plasmid was provided by D. Thanos (Academy of Athens, Athens, Greece). FLAG-RIG-I and FLAG-RIG-I-CARD were provided by C. Basler. FLAG-MAVS was provided by K. Li (University of Tennessee, Memphis, TN). FLAG-TBK1 was provided by S. Sun (MD Anderson Cancer Center, Houston, TX). FLAG-A20 WT, FLAG-A20 C103A mutant, and FLAG-A20 ZnF4 mutant were provided by C. Vincenz (University of Michigan, Ann Arbor, MI) and E.W. Harhaj (Johns Hopkins School of Medicine), HA-TRIM25 was purchased from Addgene Inc. 37 human USPs cDNA clones were purchased from Open Biosystems Company and subcloned into pcDNA3.1 expression vector (Invitrogen, CA) as described previously (Fan et al., 2011). Mammalian expression vectors for USP21 WT and C221A mutant with or without an N-terminal MYC or FLAG tag were described previously (Xu et al., 2010). Expression vectors for CYLD and A20 were described previously (Fan et al., 2011).

Transfection and reporter gene assays. HEK293T cells and MEF cells were transfected with expression plasmids using FuGene 6 (Roche) or Lipofectamine 2000 respectively (Invitrogen). Reporter gene assays were performed as described previously (Fan et al., 2010). In brief, targeted cells were seeded at a concentration of 3×10^5 cells per well and cultured overnight in 6-well plates. The cells were transfected with the indicated plasmids, together with IFN-β, ISRE, NF-κB–dependent *firefly* luciferase construct and *Renilla* luciferase construct.

Immunoblot analysis, coimmunoprecipitation, and quantitative RT-PCR. These experiments were performed as previously described (Fan et al., 2010). In brief, targeted cells were lysed in lysate buffer (25 mM Tris-HCl, pH 7.4, 150 mM NaCl, 1 mM EDTA, 1% NP-40 and 5% glycerol, 1 mM PMSF, 1 mM DTT, 10 μg/ml aprotinin, 10 μg/ml leupeptin, 1 mM benzamidine, and phosphatase inhibitor cocktail A and B). After centrifuging cell lysate at 15,000 *g* for 15 min at 4°C, primary antibodies were added to the supernatant and incubated with rotation for 3 h at 4°C. After adding a protein A–agarose bead suspension, the mixture was further incubated with rotation for 3 h at 4°C. The precipitates were washed three times using precold washing buffer (20 mM Hepes, pH 7.7, 50 mM NaCl, 2.5 mM $MgCl_2$, 0.1 mM EDTA, and 0.05% Triton X-100), and then the beads were resuspended in Laemmli sample buffer and boiled for 10 min. For RT-PCR, cells were collected using TRIzol (Invitrogen) and RNA extracted according to manufacturer's protocol. Quantitative real-time PCR was performed using KAPA SYBR FAST Universal one-Step qRT-PCR kit (ABgene) and analyzed by Applied Biosystems 7300 real-time PCR system. Data were normalized to housekeeping GAPDH or 18S gene and the relative abundance of the transcripts was calculated by the Ct models.

Immunofluorescent confocal microscopy. Cells were grown on Chamber slide, and uninfected or infected with SeV for 8 h. Treated cells were fixed in 4% paraformaldehyde for 15 min, permeabilized by 0.2% Triton X-100, and then blocked with 1% BSA for 45 min. Primarily antibodies were incubated overnight at 4°C. After washing three times, the cells were probed with

fluorescently conjugated secondary antibodies for 1 h at room temperature, and followed by blue nuclear counterstaining with Hoechst. Coverslips were mounted and observed with an Olympus Fluoview FV 1000 Laser Scan Confocal Microscope.

In vitro deubiquitination assay. MYC-USP21-WT, MYC-USP21-C221A, MYC-CYLD, or MYC-A20 proteins were expressed in HEK293T cells and immunoprecipitated by MYC antibodies. To perform in vitro deubiquitination assay, FLAG-RIG-I-CARD expression vectors were transfected into HEK293T cells with the vectors encoding HA-Ub. Cells were lysed in the lysis buffer only with PMSF as a protease inhibitor and centrifuged at 15,000 *g* for 15 min. Supernatant containing polyubiquitinated FLAG-RIG-I-CARD proteins in the cell lysates were co-incubated with the immunoprecipitated MYC-USP21 WT or C221A mutant for 2 h at 30°C. After reaction, 0.1% SDS would be added and FLAG-RIG-I-CARD proteins in the supernatant were immunoprecipitated with anti-FLAG antibodies and immunoblotted with anti-HA antibodies to detect the presence of ubiquitinated FLAG-RIG-I-CARD.

Viruses. SeV was purchased from Charles River. VSV and VSV-eGFP were gifts from G. Barber (University of Miami. Miami, FL). VSV was generated and titrated on baby hamster kidney (BHK21) cells or Vero cells, respectively. In brief, BHK21 cells were infected with VSV until >70% of cells exhibited clear cytopathic effects. Cell supernatant was harvested and separated into aliquots at −80°C. To titer VSV, Vero cells were seeded into a 6-well plate at 8×10^5 cells per well. At the next day, serial dilutions of the stocked virus were made in DMEM without serum. Diluted virus suspension was then added to Vero cells. After 1 h of incubation at 37°C, viruses were removed. Subsequently, wells were overlaid with 2 ml of growth medium with 1% of low-melting agarose and incubated at 37°C for 10 d. The viral titer was estimated by counting the plaque number.

Viral infection in mice and measurement of IFN production. Mice of different genotypes were infected with VSV via intraperitoneal or tail vein injection. Sera were collected at different time points for measuring IFN induction by ELISA according to the manufacturer's instructions. ELISA kits for mouse IFN-α and IFN-β were purchased from PBL Biomedical Laboratories.

We are very grateful to Drs. Shao-cong Sun, Kui Li, Rongfu Wang, Dimitris Thanos, Chris Basler, Edward W. Harhaj, Claudius Vincenz, Averil Ma, Lydia Matesic, and Linjie Guo for providing the expression constructs or MEF cell lines or technical advice described in this paper.

This work was supported in part by the grants from National Institutes of Health-NINDS 1R01NS072420 and 1R21NS085467, the National Basic Research Program 2013CB967500, National Natural Science Foundation of China 31170824, the Basic Research Project of Shanghai Science and Technology Commission 13JC1405400, the Specialized Research Fund for the Doctoral Program of Higher Education 20120072110016.

Submitted: 25 December 2012
Accepted: 6 January 2014

REFERENCES

Akira, S., S. Uematsu, and O. Takeuchi. 2006. Pathogen recognition and innate immunity. *Cell*. 124:783–801. http://dx.doi.org/10.1016/j.cell.2006.02.015

Bhoj, V.G., and Z.J. Chen. 2009. Ubiquitylation in innate and adaptive immunity. *Nature*. 458:430–437. http://dx.doi.org/10.1038/nature07959

Fan, Y.H., Y. Yu, Y. Shi, W.J. Sun, M. Xie, N. Ge, R.F. Mao, A. Chang, G. Xu, M.D. Schneider, et al. 2010. Lysine 63-linked polyubiquitination of TAK1 at lysine 158 is required for tumor necrosis factor alpha- and interleukin-1 beta-induced IKK/NF-kappaB and JNK/AP-1 activation. *J. Biol. Chem.* 285:5347–5360. http://dx.doi.org/10.1074/jbc.M109.076976

Fan, Y.H., Y. Yu, R.F. Mao, X.J. Tan, G.F. Xu, H. Zhang, X.B. Lu, S.B. Fu, and J. Yang. 2011. USP4 targets TAK1 to downregulate TNFα-induced NF-κB activation. *Cell Death Differ.* 18:1547–1560. http://dx.doi.org/10.1038/cdd.2011.11

Friedman, C.S., M.A. O'Donnell, D. Legarda-Addison, A. Ng, W.B. Cárdenas, J.S. Yount, T.M. Moran, C.F. Basler, A. Komuro, C.M. Horvath, et al. 2008. The tumour suppressor CYLD is a negative regulator of RIG-I-mediated antiviral response. *EMBO Rep.* 9:930–936. http://dx.doi.org/10.1038/embor.2008.136

Fujita, T. 2009. A nonself RNA pattern: tri-p to panhandle. *Immunity*. 31:4–5. http://dx.doi.org/10.1016/j.immuni.2009.06.014

Gack, M.U., Y.C. Shin, C.H. Joo, T. Urano, C. Liang, L. Sun, O. Takeuchi, S. Akira, Z. Chen, S. Inoue, and J.U. Jung. 2007. TRIM25 RING-finger E3 ubiquitin ligase is essential for RIG-I-mediated antiviral activity. *Nature*. 446:916–920. http://dx.doi.org/10.1038/nature05732

Gack, M.U., A. Kirchhofer, Y.C. Shin, K.S. Inn, C. Liang, S. Cui, S. Myong, T. Ha, K.P. Hopfner, and J.U. Jung. 2008. Roles of RIG-I N-terminal tandem CARD and splice variant in TRIM25-mediated antiviral signal transduction. *Proc. Natl. Acad. Sci. USA*. 105:16743–16748. http://dx.doi.org/10.1073/pnas.0804947105

Gao, D., Y.K. Yang, R.P. Wang, X. Zhou, F.C. Diao, M.D. Li, Z.H. Zhai, Z.F. Jiang, and D.Y. Chen. 2009. REUL is a novel E3 ubiquitin ligase and stimulator of retinoic-acid-inducible gene-I. *PLoS ONE*. 4:e5760. http://dx.doi.org/10.1371/journal.pone.0005760

García-Santisteban, I., S. Bañuelos, and J.A. Rodríguez. 2012. A global survey of CRM1-dependent nuclear export sequences in the human deubiquitinase family. *Biochem. J.* 441:209–217. http://dx.doi.org/10.1042/BJ20111300

Honda, K., A. Takaoka, and T. Taniguchi. 2006. Type I interferon [corrected] gene induction by the interferon regulatory factor family of transcription factors. *Immunity*. 25:349–360. http://dx.doi.org/10.1016/j.immuni.2006.08.009

Kato, H., S. Sato, M. Yoneyama, M. Yamamoto, S. Uematsu, K. Matsui, T. Tsujimura, K. Takeda, T. Fujita, O. Takeuchi, and S. Akira. 2005. Cell type-specific involvement of RIG-I in antiviral response. *Immunity*. 23:19–28. http://dx.doi.org/10.1016/j.immuni.2005.04.010

Kato, H., O. Takeuchi, S. Sato, M. Yoneyama, M. Yamamoto, K. Matsui, S. Uematsu, A. Jung, T. Kawai, K.J. Ishii, et al. 2006. Differential roles of MDA5 and RIG-I helicases in the recognition of RNA viruses. *Nature*. 441:101–105. http://dx.doi.org/10.1038/nature04734

Kawai, T., K. Takahashi, S. Sato, C. Coban, H. Kumar, H. Kato, K.J. Ishii, O. Takeuchi, and S. Akira. 2005. IPS-1, an adaptor triggering RIG-I- and Mda5-mediated type I interferon induction. *Nat. Immunol.* 6:981–988. http://dx.doi.org/10.1038/ni1243

Kayagaki, N., Q. Phung, S. Chan, R. Chaudhari, C. Quan, K.M. O'Rourke, M. Eby, E. Pietras, G. Cheng, J.F. Bazan, et al. 2007. DUBA: a deubiquitinase that regulates type I interferon production. *Science*. 318:1628–1632. http://dx.doi.org/10.1126/science.1145918

Komander, D., M.J. Clague, and S. Urbé. 2009. Breaking the chains: structure and function of the deubiquitinases. *Nat. Rev. Mol. Cell Biol.* 10:550–563. http://dx.doi.org/10.1038/nrm2731

Lin, R., L. Yang, P. Nakhaei, Q. Sun, E. Sharif-Askari, I. Julkunen, and J. Hiscott. 2006. Negative regulation of the retinoic acid-inducible gene I-induced antiviral state by the ubiquitin-editing protein A20. *J. Biol. Chem.* 281:2095–2103. http://dx.doi.org/10.1074/jbc.M510326200

Malakhova, O.A., K.I. Kim, J.K. Luo, W. Zou, K.G. Kumar, S.Y. Fuchs, K. Shuai, and D.E. Zhang. 2006. UBP43 is a novel regulator of interferon signaling independent of its ISG15 isopeptidase activity. *EMBO J.* 25:2358–2367. http://dx.doi.org/10.1038/sj.emboj.7601149

Meylan, E., J. Curran, K. Hofmann, D. Moradpour, M. Binder, R. Bartenschlager, and J. Tschopp. 2005. Cardif is an adaptor protein in the RIG-I antiviral pathway and is targeted by hepatitis C virus. *Nature*. 437:1167–1172. http://dx.doi.org/10.1038/nature04193

Moser, K.L., J.A. Kelly, C.J. Lessard, and J.B. Harley. 2009. Recent insights into the genetic basis of systemic lupus erythematosus. *Genes Immun.* 10:373–379. http://dx.doi.org/10.1038/gene.2009.39

Nakagawa, T., T. Kajitani, S. Togo, N. Masuko, H. Ohdan, Y. Hishikawa, T. Koji, T. Matsuyama, T. Ikura, M. Muramatsu, and T. Ito. 2008. Deubiquitylation of histone H2A activates transcriptional initiation via trans-histone cross-talk with H3K4 di- and trimethylation. *Genes Dev.* 22:37–49. http://dx.doi.org/10.1101/gad.1609708

Nijman, S.M., M.P. Luna-Vargas, A. Velds, T.R. Brummelkamp, A.M. Dirac, T.K. Sixma, and R. Bernards. 2005. A genomic and functional inventory of deubiquitinating enzymes. *Cell*. 123:773–786. http://dx.doi.org/10.1016/j.cell.2005.11.007

Oshiumi, H., M. Matsumoto, S. Hatakeyama, and T. Seya. 2009. Riplet/RNF135, a RING finger protein, ubiquitinates RIG-I to promote interferon-beta induction during the early phase of viral infection. *J. Biol. Chem.* 284:807–817. http://dx.doi.org/10.1074/jbc.M804259200

Oshiumi, H., M. Miyashita, N. Inoue, M. Okabe, M. Matsumoto, and T. Seya. 2010. The ubiquitin ligase Riplet is essential for RIG-I-dependent innate immune responses to RNA virus infection. *Cell Host Microbe*. 8:496–509. http://dx.doi.org/10.1016/j.chom.2010.11.008

Parvatiyar, K., G.N. Barber, and E.W. Harhaj. 2010. TAX1BP1 and A20 inhibit antiviral signaling by targeting TBK1-IKKi kinases. *J. Biol. Chem.* 285:14999–15009. http://dx.doi.org/10.1074/jbc.M110.109819

Ramos, P.S., A.H. Williams, J.T. Ziegler, M.E. Comeau, R.T. Guy, C.J. Lessard, H. Li, J.C. Edberg, R. Zidovetzki, L.A. Criswell, et al. 2011. Genetic analyses of interferon pathway-related genes reveal multiple new loci associated with systemic lupus erythematosus. *Arthritis Rheum.* 63:2049–2057. http://dx.doi.org/10.1002/art.30356

Ritchie, K.J., C.S. Hahn, K.I. Kim, M. Yan, D. Rosario, L. Li, J.C. de la Torre, and D.E. Zhang. 2004. Role of ISG15 protease UBP43 (USP18) in innate immunity to viral infection. *Nat. Med.* 10:1374–1378. http://dx.doi.org/10.1038/nm1133

Saitoh, T., M. Yamamoto, M. Miyagishi, K. Taira, M. Nakanishi, T. Fujita, S. Akira, N. Yamamoto, and S. Yamaoka. 2005. A20 is a negative regulator of IFN regulatory factor 3 signaling. *J. Immunol.* 174:1507–1512.

Satoh, T., H. Kato, Y. Kumagai, M. Yoneyama, S. Sato, K. Matsushita, T. Tsujimura, T. Fujita, S. Akira, and O. Takeuchi. 2010. LGP2 is a positive regulator of RIG-I- and MDA5-mediated antiviral responses. *Proc. Natl. Acad. Sci. USA*. 107:1512–1517. http://dx.doi.org/10.1073/pnas.0912986107

Seth, R.B., L. Sun, C.K. Ea, and Z.J. Chen. 2005. Identification and characterization of MAVS, a mitochondrial antiviral signaling protein that activates NF-kappaB and IRF 3. *Cell*. 122:669–682. http://dx.doi.org/10.1016/j.cell.2005.08.012

Shembade, N., N.S. Harhaj, D.J. Liebl, and E.W. Harhaj. 2007. Essential role for TAX1BP1 in the termination of TNF-alpha-, IL-1- and LPS-mediated NF-kappaB and JNK signaling. *EMBO J.* 26:3910–3922. http://dx.doi.org/10.1038/sj.emboj.7601823

Shembade, N., N.S. Harhaj, K. Parvatiyar, N.G. Copeland, N.A. Jenkins, L.E. Matesic, and E.W. Harhaj. 2008. The E3 ligase Itch negatively regulates inflammatory signaling pathways by controlling the function of the ubiquitin-editing enzyme A20. *Nat. Immunol.* 9:254–262. http://dx.doi.org/10.1038/ni1563

Shembade, N., K. Parvatiyar, N.S. Harhaj, and E.W. Harhaj. 2009. The ubiquitin-editing enzyme A20 requires RNF11 to downregulate NF-kappaB signalling. *EMBO J.* 28:513–522. http://dx.doi.org/10.1038/emboj.2008.285

Shembade, N., A. Ma, and E.W. Harhaj. 2010. Inhibition of NF-kappaB signaling by A20 through disruption of ubiquitin enzyme complexes. *Science*. 327:1135–1139. http://dx.doi.org/10.1126/science.1182364

Takeuchi, O., and S. Akira. 2010. Pattern recognition receptors and inflammation. *Cell*. 140:805–820. http://dx.doi.org/10.1016/j.cell.2010.01.022

Urbé, S., H. Liu, S.D. Hayes, C. Heride, D.J. Rigden, and M.J. Clague. 2012. Systematic survey of deubiquitinase localization identifies USP21 as a regulator of centrosome- and microtubule-associated functions. *Mol. Biol. Cell*. 23:1095–1103. http://dx.doi.org/10.1091/mbc.E11-08-0668

Wang, Y.Y., L. Li, K.J. Han, Z. Zhai, and H.B. Shu. 2004. A20 is a potent inhibitor of TLR3- and Sendai virus-induced activation of NF-kappaB and ISRE and IFN-beta promoter. *FEBS Lett.* 576:86–90. http://dx.doi.org/10.1016/j.febslet.2004.08.071

Wertz, I.E., and V.M. Dixit. 2010. Signaling to NF-kappaB: regulation by ubiquitination. *Cold Spring Harb. Perspect. Biol.* 2:a003350. http://dx.doi.org/10.1101/cshperspect.a003350

Wertz, I.E., K.M. O'Rourke, H. Zhou, M. Eby, L. Aravind, S. Seshagiri, P. Wu, C. Wiesmann, R. Baker, D.L. Boone, et al. 2004. De-ubiquitination and ubiquitin ligase domains of A20 downregulate NF-kappaB signalling. *Nature*. 430:694–699. http://dx.doi.org/10.1038/nature02794

Xia, Z.P., L. Sun, X. Chen, G. Pineda, X. Jiang, A. Adhikari, W. Zeng, and Z.J. Chen. 2009. Direct activation of protein kinases by unanchored polyubiquitin chains. *Nature*. 461:114–119. http://dx.doi.org/10.1038/nature08247

Xu, L.G., Y.Y. Wang, K.J. Han, L.Y. Li, Z. Zhai, and H.B. Shu. 2005. VISA is an adapter protein required for virus-triggered IFN-beta signaling. *Mol. Cell*. 19:727–740. http://dx.doi.org/10.1016/j.molcel.2005.08.014

Xu, G., X. Tan, H. Wang, W. Sun, Y. Shi, S. Burlingame, X. Gu, G. Cao, T. Zhang, J. Qin, and J. Yang. 2010. Ubiquitin-specific peptidase 21 inhibits tumor necrosis factor alpha-induced nuclear factor kappaB activation via binding to and deubiquitinating receptor-interacting protein 1. *J. Biol. Chem.* 285:969–978. http://dx.doi.org/10.1074/jbc.M109.042689

Yamazaki, K., J. Gohda, A. Kanayama, Y. Miyamoto, H. Sakurai, M. Yamamoto, S. Akira, H. Hayashi, B. Su, and J. Inoue. 2009. Two mechanistically and temporally distinct NF-kappaB activation pathways in IL-1 signaling. *Sci. Signal*. 2:ra66. http://dx.doi.org/10.1126/scisignal.2000387

Ye, Y., M. Akutsu, F. Reyes-Turcu, R.I. Enchev, K.D. Wilkinson, and D. Komander. 2011. Polyubiquitin binding and cross-reactivity in the USP domain deubiquitinase USP21. *EMBO Rep.* 12:350–357. http://dx.doi.org/10.1038/embor.2011.17

Yoneyama, M., and T. Fujita. 2009. RNA recognition and signal transduction by RIG-I-like receptors. *Immunol. Rev.* 227:54–65. http://dx.doi.org/10.1111/j.1600-065X.2008.00727.x

Yoneyama, M., M. Kikuchi, T. Natsukawa, N. Shinobu, T. Imaizumi, M. Miyagishi, K. Taira, S. Akira, and T. Fujita. 2004. The RNA helicase RIG-I has an essential function in double-stranded RNA-induced innate antiviral responses. *Nat. Immunol.* 5:730–737. http://dx.doi.org/10.1038/ni1087

Zeng, W., M. Xu, S. Liu, L. Sun, and Z.J. Chen. 2009. Key role of Ubc5 and lysine-63 polyubiquitination in viral activation of IRF3. *Mol. Cell*. 36:315–325. http://dx.doi.org/10.1016/j.molcel.2009.09.037

Zeng, W., L. Sun, X. Jiang, X. Chen, F. Hou, A. Adhikari, M. Xu, and Z.J. Chen. 2010. Reconstitution of the RIG-I pathway reveals a signaling role of unanchored polyubiquitin chains in innate immunity. *Cell*. 141:315–330. http://dx.doi.org/10.1016/j.cell.2010.03.029

Zhang, M., X. Wu, A.J. Lee, W. Jin, M. Chang, A. Wright, T. Imaizumi, and S.C. Sun. 2008. Regulation of IkappaB kinase-related kinases and antiviral responses by tumor suppressor CYLD. *J. Biol. Chem.* 283:18621–18626. http://dx.doi.org/10.1074/jbc.M801451200

Zhang, M., A.J. Lee, X. Wu, and S.C. Sun. 2011. Regulation of antiviral innate immunity by deubiquitinase CYLD. *Cell. Mol. Immunol.* 8:502–504. http://dx.doi.org/10.1038/cmi.2011.42